

1                   **Investigation of isoprene dynamics during the**  
2                   **day-to-night transition period**

3                   **Dandan Wei<sup>1</sup>, Hariprasad D. Alwe<sup>2</sup>, Dylan B. Millet<sup>2</sup>, Sarah C. Kavassalis<sup>3</sup>,**  
4                   **Michelle Lew<sup>4</sup>, Brandon Bottorff<sup>4</sup>, Philip S. Stevens<sup>4,5</sup>, Allison L. Steiner<sup>1</sup>**

5                   <sup>1</sup>Department of Climate and Space Sciences and Engineering, University of Michigan, Ann Arbor,  
6                   Michigan, USA

7                   <sup>2</sup>Department of Soil, Water and Climate, University of Minnesota, St. Paul, Minnesota, USA

8                   <sup>3</sup>Department of Chemistry, University of Toronto, Ontario, Canada

9                   <sup>4</sup>Department of Chemistry, Indiana University, Bloomington, Indiana, USA

10                  <sup>5</sup>School of Public and Environmental Affairs, Indiana University, Bloomington, Indiana, USA

- 11                  1. Low turbulent mixing during clear and calm nights leads to accumulation of iso-  
12                  prene within the canopy
- 13                  2. Turbulent mixing accounts for 80% of the observed nighttime isoprene loss rates
- 14                  3. Isoprene flux measurements did not capture the majority of the removal of the ac-  
15                  cumulated isoprene

This is the author manuscript accepted for publication and has undergone full peer review but has not been through the copyediting, typesetting, pagination and proofreading process, which may lead to differences between this version and the [Version of Record](#). Please cite this article as doi: [10.1029/2020JD032784](https://doi.org/10.1029/2020JD032784)

Corresponding author: Dandan Wei, [dandanwe@umich.edu](mailto:dandanwe@umich.edu)

**Abstract**

At the University of Michigan Biological Station during the 2016 AMOS field campaign, isoprene concentrations typically peak in the early afternoon (around 15:00 local time, LT) under well-mixed conditions. However, an end-of-day peak (around 21:00 LT) occurs on 23% of the campaign days, followed by a rapid removal (from 21:00 - 22:00 LT) at rate of  $0.57 \text{ hr}^{-1}$  during the day-to-night transition period. During the end-of-day peak, in-canopy isoprene concentrations increase by 77% (from 3.5 ppbv to 6.2 ppbv) on average. Stratification and weak winds ( $< 3.4 \text{ m s}^{-1}$  at 46 m) significantly suppress turbulent exchanges between in- and above-canopy, leading to accumulation of isoprene emitted at dusk. A critical standard deviation of the vertical velocity ( $\sigma_w$ ) of 0.14, 0.2, and  $0.29 \text{ m s}^{-1}$  is identified to detect the end-of-day peak for the height of 13, 21, and 34 m, respectively. In 85% of the end-of-day cases, the wind speed increases above  $2.5 \text{ m s}^{-1}$  after the peak along with a shift in wind direction, and turbulence is re-established. Therefore, the wind speed of  $2.5 \text{ m s}^{-1}$  is considered as the threshold point where turbulence switches from being independent of wind speed to dependent on wind speed. The reinstated turbulence accounts for 80% of the subsequent isoprene removal with the remaining 20% explained by chemical reactions with hydroxyl radicals, ozone, and nitrate radicals. Observed isoprene fluxes do not support the argument that the end-of-day peak is reduced by vertical turbulent mixing, and we hypothesize that horizontal advection may play a role.

## 1 Introduction

Isoprene accounts for almost half of the non-methane biogenic volatile organic compound (BVOCs) fluxes emitted to the atmosphere globally (Guenther et al., 2012). Isoprene substantially influences hydroxyl radical (OH) concentration in the atmosphere and thus atmospheric oxidative capacity and tropospheric chemistry (Taraborrelli et al., 2012; Fuchs et al., 2013). In addition, because of the large flux of isoprene into the atmosphere (Guenther et al. 2012), oxidation of isoprene is a significant source of secondary organic aerosols (SOA) with implication for air quality and climate (Claeys, 2004; Robinson et al., 2011). While daytime isoprene has been studied thoroughly, its day-to-night transition has received little attention. The near-zero emissions during the transition period allow us to better quantify processes responsible for isoprene loss, which is critical for accurate estimation of nighttime chemistry and SOA formation (especially nitrate SOA; Ng et al. 2008).

Daytime isoprene concentrations shows pronounced diurnal cycles with a peak in the early afternoon (around 15:00 local time) in response to sources (e.g. emission) and sinks (e.g. turbulent mixing and chemical reactions). Isoprene emission from plants is linked to photosynthesis and thus highly temperature- and light-dependent. As a result, isoprene emission peaks around noon and shuts down after sunset (Guenther et al., 1993). After being emitted into the atmosphere, isoprene is redistributed by turbulent mixing and at the same time chemically consumed by OH, ozone ( $O_3$ ), and nitrate radicals ( $NO_3$ ). Since the  $O_3$  reaction is slow ( $\tau = 30$  h at  $[O_3] = 30$  ppbv) and  $NO_3$  mainly exists at night, OH is considered to be the major chemical sink of isoprene during the daytime (Levy, 1971; Lelieveld et al., 2008). OH is photolytically produced and its concentrations drop significantly at sunset due to reduced radiation. Given that the loss of isoprene to OH diminishes towards the end of the day ( $\tau = 11.5$  hours at  $[OH] = 2.42 \times 10^5$  molecules  $cm^{-3}$ , 2016 AMOS campaign average for 19:00 local time), turbulent mixing of isoprene emitted close to dusk plays an important role in shaping the nocturnal isoprene mixing ratios.

An End-Of-Day (EOD) peak was frequently observed around 21:00 local time (LT) during the AMOS (Atmospheric Measurements of Oxidants in Summer) field campaign, followed by a precipitous decay in isoprene from 21:00 - 22:00 LT (Fig. 1a). In this study, we aim to (i) characterize the EOD peak and understand its origin and (ii) constrain the possible mechanisms responsible for the rapid decline in isoprene. As for the EOD peak, previous field studies have reported elevated surface isoprene concentrations during the early evening in various locations (Martin et al., 1991; Montzka et al., 1993; Goldan et al., 1995; Starn et al., 1998). Martin et al. (1991) observed that peak isoprene concentrations at Scotia, Pennsylvania, occurred at 20:00 local time, at levels 2-3 times those observed at noon. Starn et al. (1998) interpreted elevated isoprene concentrations as a result of

71 advective transport to the measurement site. But little quantitative explanations for the  
72 EOD isoprene peak are provided by previous studies. As for the subsequent decay, rapid  
73 isoprene removal during the day-to-night transition period has been frequently observed in  
74 forested environments. Due to the lack of constraints from reliable measurements, the cause  
75 of this rapid decrease in isoprene has been attributed to chemical loss (Faloona et al., 2001)  
76 or dynamics (Sillman et al., 2002; Apel, 2002). Hurst et al. (2001) estimated that either OH  
77 or vertical mixing could be the reason for this phenomenon, but no direct measurements  
78 were available to differentiate the two processes. Faloona et al. (2001) observed abnormally  
79 high OH concentrations at night, suggesting OH was responsible for the rapid decay in  
80 isoprene, but interferences for this OH instrument were later reported (Feiner et al., 2016).  
81 Apel (2002) and Sillman et al. (2002) postulated vertical dilution or horizontal advection  
82 could explain the rapid removal, but no turbulence data existed to support the speculation.

83 During the day-to-night transition period, organization of canopy flows in forested sites  
84 falls into two major categories: (i) well-mixed conditions where the turbulence is continuous  
85 down to the ground; (ii) more stable conditions as the canopy begins to cool, characterized  
86 by a temperature inversion and turbulence suppressed on all scales (Mahrt, 1999). On clear  
87 and calm nights, thermal stratification and weak mechanical production of turbulence favor  
88 the generation of such stable conditions (B. Van de Wiel et al., 2012; Van de Wiel et al.,  
89 2012) under which the above- and in-canopy air layer exchanges are significantly weakened  
90 (commonly known as decoupling). Early-evening decoupling has been observed frequently  
91 (at least 31% of the summer nighttime periods, Alekseychik et al. 2013) at various forested  
92 sites (Burns et al., 2010; van Gorsel et al., 2011; Alekseychik et al., 2013; Oliveira et al.,  
93 2012). Smaller biogenic fluxes and larger gradients in temperature and scalar concentration  
94 between above- and in-canopy layers coincide with decoupling conditions due to reduced  
95 mixing (Alekseychik et al., 2013; Oliveira et al., 2012).

96 However, overnight turbulence generation can lead to a breakdown of the decoupling  
97 state, allowing for re-coupling and mixing between the canopy interior and the air above  
98 it (Oliveira et al., 2012; Alekseychik et al., 2013). During the aforementioned decoupling  
99 period, nonstationary motions (such as density currents, drainage flow, and canopy waves)  
100 dominate (Mahrt et al., 2012; Sun et al., 2012) and turbulence is weak, intermittent and  
101 independent of the mean wind speed (Liang et al., 2014). However, evidence suggests  
102 that there is a "threshold" point at which stable-condition turbulence switches from being  
103 independent of wind speed to being dependent on wind speed (Mahrt et al., 2012; Sun et  
104 al., 2012; Liang et al., 2014). The resultant wind-induced turbulence significantly affects  
105 the nighttime vertical profile of scalars as well as scalar flux determination (Oliveira et al.,

106 2012). Therefore, wind speed and the resultant turbulence are then expected to influence  
107 the vertical gradient of isoprene during the transition period.

108 The 2016 AMOS campaign at UMBS (University of Michigan Biological Station) provide  
109 detailed measurements of isoprene and its oxidants (i.e. OH, NO<sub>3</sub>, O<sub>3</sub>) as well as  
110 meteorological and turbulence data, which allow us to fill in the gaps in our knowledge of  
111 the chemical and physical processes governing isoprene dynamics during the day-to-night  
112 transition period. In the present study, we compare two distinct isoprene patterns during  
113 the transition period to show the characteristics and origin of the EOD isoprene peak. We  
114 also discuss and constrain possible mechanisms for the subsequent isoprene removal to il-  
115 luminate the relative importance of turbulence and chemistry on nocturnal distribution of  
116 reactive gases in forested environment.

## 117 2 Methods

### 118 2.1 Study site

119 The 2016 AMOS (Atmospheric Measurements of Oxidants in Summer) field campaign  
120 was conducted in the UMBS (University of Michigan Biological Station) site located near  
121 the northern end of the lower peninsula of Michigan, US during the month of July. The  
122 UMBS site is a mixed deciduous/coniferous forest and isoprene-dominated (Millet et al.,  
123 2018). It is surrounded by the Great Lakes, with Lake Superior 21 km to the north, Lake  
124 Michigan 35 km to the west, and Lake Huron 42 km to the east. In addition, there are  
125 smaller lakes scattered within 3 km of the site. For example, Douglas lake is less than 200  
126 meters to the north of the UMBS site and Burt Lake is about 2.5 km south of the site. There  
127 was little indication of local anthropogenic pollution in the surrounding area during the field  
128 campaign (NO<sub>x</sub> < 0.1 ppbv), although the region is frequently impacted by the transport of  
129 NO<sub>x</sub> from urban areas to the south and west (e.g., Milwaukee, Chicago, Detroit; Cooper  
130 et al., 2001; VanReken et al., 2015) as well as long-range transport of smoke pollution from  
131 Canada (Cooper et al., 2001; Gunsch et al., 2018). The 31 m PROPHET (Program for  
132 Research on Oxidants: PHotochemistry, Emissions, and Transport) tower extends to 34 m  
133 with a triangle tower on top. The canopy height surrounding the tower is about 22.5 m.

### 134 2.2 Measurements

135 Turbulence data (10 Hz) were collected at 5 heights on the PROPHET tower: 34 m  
136 (CSAT 3B, Campbell Scientific Inc.), 29 m (81000, RM Young), 21 m (CSAT 3, Campbell  
137 Scientific Inc.), 13m (CSAT 3, Campbell Scientific Inc.), and 5 m (CSAT 3, Campbell  
138 Scientific Inc.). High-frequency data outside of 3.5-standard deviations were removed and

139 data then were separated into 30-minute windows to apply a tilt correction (Foken, 2009).  
140 The 30-minute periods that experienced rain (as measured by the rain-gauge at the UMBS  
141 AmeriFlux tower), weak winds ( $< 0.5 \text{ m s}^{-1}$  at the top sonic anemometer), and wind  
142 directed through the tower were excluded due to potential interference. Other meteorological  
143 measurements (at 46 m) used here include photosynthetic photon flux densities (PPFD)  
144 measured at the US-UMB Ameriflux tower (about 130 m from the PROPHET tower) using  
145 a BF5 Sunshine Sensor (Delta-T Devices Ltd.), air temperature measured with a Vaisala  
146 HMP-60 in a 6-plate radiation shield at the top of the PROPHET tower, and wind speed  
147 and direction.

148 Measurements of isoprene and other VOCs were performed by PTR-QiTOF (Ionicon  
149 Analytik, GmbH) from 6 sampling heights on the PROPHET tower: 34, 21, 17, 13, 9,  
150 and 5 m (Millet et al., 2018; Alwe et al., 2019). The measurement sequence cycled hourly  
151 between these inlets using a custom-built automated sampling manifold, with 30 min per  
152 hour spent sampling from the 34 m inlet and 5 min per hour from the remaining five inlets.  
153 The remaining 5 min of each hour was used to perform a measurement blank. It is therefore  
154 an approximation to treat the vertical gradient of isoprene as a complete gradient at a  
155 single point in time, because it reflects sequential measurements. Thirty days of isoprene  
156 data were obtained. We excluded the cloudy and rainy days, and identified 7 cases with  
157 end-of-day peaks and 7 cases with early-afternoon peaks (hereafter referred to as standard  
158 cases). Turbulence measurements performed at the 34 m isoprene sampling inlet were used  
159 to compute hourly isoprene fluxes. Details of the isoprene measurements and calibration  
160 can be found in Millet et al. (2018).

161 Other chemical measurements at the PROPHET tower implemented in this study in-  
162 clude OH (hydroxyl radical) and  $\text{O}_3$  (ozone) concentrations.  $\text{O}_3$  were measured at 6 m using  
163 a Model 205 (2B Technologies, Inc.) dual-beam UV absorption instrument. OH radicals  
164 were measured at the top of the PROPHET tower at a height of 32 m using the Indiana  
165 University Laser-Induced Fluorescence - Fluorescence Assay by Gas Expansion (LIF-FAGE)  
166 instrument (Dusanter et al., 2009). To quantify potential interferences during ambient mea-  
167 surements of OH, perfluoropropylene ( $\text{C}_3\text{F}_6$ ) was added above the sampling nozzle using an  
168 automated injector to chemically remove ambient OH radicals (Griffith et al., 2016; Rickly  
169 & Stevens, 2018). Any signal measured during  $\text{C}_3\text{F}_6$  addition thus provided a quantification  
170 of instrumental interferences. During PROPHET-AMOS, no unknown interferences were  
171 detected during the campaign using this method.

## 2.3 Data analysis

### 2.3.1 Virtual potential temperature

Virtual potential temperature ( $\theta_v$ ) was calculated using the equation below:

$$\theta_v = T_v \left( \frac{p_0}{p} \right)^\kappa \quad (1)$$

where  $T_v$  is the virtual temperature,  $p_0$  is the standard pressure at sea level (1013.25 hPa),  $p$  is the air pressure at the height of  $T_v$ , and  $\kappa$  is the Poisson constant (0.2854). In the present study, we used the sonic temperature ( $T_s$ ) from the sonic anemometers as the virtual temperature ( $T_v$ ) because they are almost equal (Rebmann et al., 2011). Two levels of pressure data (6 m and 34 m) are available. The 6 m pressure data was used for the calculations of  $\theta_v$  within the canopy (at 5 m, 13 m, and 21 m), and the 34 m pressure data for the above-canopy (at 29 m and 36 m) calculations.

### 2.3.2 Turbulent mixing timescale

A mass balance approach was employed to calculate the turbulent mixing timescale for isoprene. Assuming horizontal homogeneity, the mass balance for the isoprene mixing ratio can be expressed as (Freire et al., 2017):

$$\frac{\partial[\text{ISOP}]}{\partial t} = -\frac{\partial w'[\text{ISOP}]'}{\partial z} + S(z) \quad (2)$$

where  $S(z)$  is the source/sink term. An eddy diffusivity ( $K$ ) model ( $w'[\text{ISOP}]' = -K \frac{\partial[\text{ISOP}]}{\partial z}$ ) is employed in equation (2) and the term of vertical gradients in eddy diffusivity ( $\frac{\partial K}{\partial z}$ ) is neglected for simplicity and analytical tractability. The assumption of  $\frac{\partial K}{\partial z} = 0$  is imposed to the domain  $h < z < z_0$  ( $h$  is the canopy height, and  $z_0$  is the top of the stable boundary layer). Then equation (2) reduces to:

$$\frac{\partial[\text{ISOP}]}{\partial t} = -K \frac{\partial^2[\text{ISOP}]}{\partial z^2} + S(z) \quad (3)$$

The homogeneous solution ( $S = 0$ ) to equation (3) represents the time evolution of the isoprene mixing ratio due to turbulent mixing in the domain  $h < z < z_0$ . A solution subject to the initial condition  $[\text{ISOP}](z, t = 0) = 0$ , the lower boundary condition  $[\text{ISOP}](z = h, t) = [\text{ISOP}]_h$ , and the upper boundary condition of a zero isoprene flux at  $z = z_0$  is sought. In this case, the transient solution for the isoprene mixing ratio above the canopy can be expressed as Liu (2008):

$$\frac{[\text{ISOP}](z, t)}{[\text{ISOP}]_h} = 1 - \sum_{n=0}^{\infty} \frac{4}{(2n+1)\pi} \exp\left\{-\left(\frac{(2n+1)\pi}{2}\right)^2 \frac{K(z)t}{(z_0-h)^2}\right\} \sin\left[\frac{(2n+1)\pi}{2} \frac{z-h}{z_0-h}\right] \quad (4)$$

197 A height-dependent turbulent mixing time scale can be obtained from equation (4) by finding  
 198 the time required for the isoprene mixing ratio to reach a certain fraction of the imposed  
 199 value at the top of the canopy. In the present study, the turbulent mixing time scale is  
 200 defined as the time required for  $\frac{[\text{ISOP}](z)}{[\text{ISOP}]_h} = 0.95$ . This value of 0.95 was obtained using  
 201 the vertical gradients of isoprene observed in the standard (STD) case (see section 2.2) to  
 202 represent well-mixed conditions. The inverse of the turbulent mixing timescale is then used  
 203 as the isoprene loss rate associated with turbulent mixing.

### 204 3 Results

#### 205 3.1 End-of-day peak in isoprene

##### 206 3.1.1 Case studies

207 Here we define two classes of diurnal isoprene profiles: (i) the end-of-day (EOD) case  
 208 where isoprene increased at dusk (1 of the 7 identified cases displayed in Fig. 1a) and (ii)  
 209 a standard (STD) diurnal cycle (1 of the 7 identified cases displayed in Fig. 1a). In the  
 210 STD case, isoprene has a pronounced diurnal cycle with a peak in the early afternoon and a  
 211 minimum just before sunrise (Fig. 1a). This diurnal pattern of isoprene has been observed  
 212 in many forests ranging from deciduous to tropical under clear and well-mixed conditions  
 213 (Apel, 2002; Wei et al., 2018), and is well-captured by models of different scales (de Arellano  
 214 et al., 2011; Ashworth et al., 2015). During the 2016 AMOS field campaign at UMBS, an  
 215 end-of-day peak in isoprene was observed during clear and calm days. The peak occurs  
 216 around 21:00 local time (LT) when the emissions are near-zero (sunset is around 21:30 LT).  
 217 Isoprene increases by over 3 ppbv from 19:00 LT to 21:00 LT followed by a precipitous  
 218 decline in the next two hours (Fig. 1a).

219 During the daytime, air temperature in the EOD case is on average 8 °C lower than  
 220 that in the STD case (Fig. 1d), indicating less surface heating and thus weaker mixing in  
 221 the EOD case, demonstrated by the decrease in the mid-day standard deviation of vertical  
 222 velocity ( $\sigma_w$ ) by a factor of 2 (Fig. 1c). During the day-to-night transition period, both  
 223 case studies show clear (cloudless) conditions (Fig. 1b) that favor the radiative cooling  
 224 of the canopy and thus the development of a more stable boundary layer. In a stable  
 225 boundary layer, thermal stratification leads to the destruction of turbulence and therefore  
 226 turbulence production depends on wind shear (Van de Wiel et al., 2012). Van de Wiel et  
 227 al. (2012) predict that the minimum wind at the crossing level (where the wind is relatively  
 228 stationary compared to lower and higher levels, typically some decameters above the surface)



229 for sustainable turbulence at the surface is 5-7 m s<sup>-1</sup> during the day-to-night transition  
230 period. The STD case shows wind speed of 5 m s<sup>-1</sup> at 46 m that appears to be adequate  
231 to sustain turbulent mixing as demonstrated by the relatively high  $\sigma_w$  value of 0.7 m s<sup>-1</sup>  
232 throughout the evening (Fig. 1c, f). In this case, the sustained mixing dominates over  
233 the decreasing emission at dusk, leading to decreases in isoprene mixing ratios during the  
234 day-to-night transition period.

235 In the EOD case, however, wind speed is low (around 2 m s<sup>-1</sup>) and drops to almost  
236 zero at 21:00 LT when the end-of-day peak occurs (Fig. 1f), indicating little mechanical  
237 production of turbulence at the time. Consequently, the  $\sigma_w$  decreases to less than 0.1 m s<sup>-1</sup>  
238 around 21:00 LT (Fig. 1c). Therefore, we hypothesize that during clear and calm nights,  
239 stratification and weak wind suppress turbulent exchanges between the canopy and the air  
240 above (also referred to as decoupling), leading to the accumulation of isoprene emitted at  
241 dusk in the canopy. In addition to the increase in wind speed, a shift in wind direction from  
242 north to south occurs at the same time as the peak, likely influencing the rapid decline of  
243 isoprene (Fig. 1f; see section 3.3.1).

### 244 **3.1.2 Relationship between isoprene mixing ratio and $\sigma_w$**

245 To demonstrate the generality of this phenomenon, seven (seven) out of thirty days  
246 are identified as EOD (STD) case. The isoprene mixing ratio and  $\sigma_w$  are averaged over  
247 all events to show their diurnal evolution (Fig. 2). For the EOD case, in-canopy isoprene  
248 begins to increase two hours before the peak that appears at 21:00 LT (Fig. 2a). Due to the  
249 time sequencing of the gradient measurements, the actual peak time could be somewhere  
250 between 20:35 - 21:00 LT (see section 2.2). Within the two hours, the average in-canopy  
251 isoprene increases 77 % (from 3.5 ppbv to 6.2 ppbv) and the in-canopy  $\sigma_w$  decreases below  
252 0.2 m s<sup>-1</sup>, indicating that the mixing rate becomes inadequate to transport the isoprene  
253 emitted out of the canopy. Within one hour of the peak, the above-canopy isoprene (1.5z/h)  
254 starts to decrease while the in-canopy isoprene (0.9z/h) keeps increasing in response to the  
255 fact that less and less isoprene is transported out of the canopy, resulting in a significant  
256 gradient between the two layers (4 ppbv) at the time of the in-canopy EOD peak (21:00 LT;  
257 Fig. 2a). This gradient, along with the low  $\sigma_w$ , suggests the decoupling of the canopy layer  
258 from the air above and thus the accumulation of isoprene in the canopy. Note that because  
259 of the 25 minute lag time in the measurement of 1.5z/h and 0.9z/h (see section 2.2), as well  
260 as the opposite trends in isoprene concentrations of the two layers, the 4 ppbv represents  
261 the upper bound of the actual gradient. In the STD case, however, no substantial gradients  
262 (< 1 ppbv) between the above- and in-canopy isoprene is observed at the time of the EOD

263 peak (21:00 LT), and  $\sigma_w$  above the canopy and in the upper canopy is generally greater  
264 than  $0.4 \text{ m s}^{-1}$ , indicating stronger vertical mixing than the EOD case.

265 Isoprene is well-mixed throughout the entire canopy during the day-to-night transition  
266 period for both EOD and STD cases (Fig. 2a, b). The large differences in  $\sigma_w$  between the  
267 two cases (Fig. 2c, d) suggest the well-mixed conditions are driven by different processes.  
268 For the STD case, no significant decrease in  $\sigma_w$  was observed even after the sunset, indicating  
269 that turbulence is continuous through the day-to-night transition, leading to a well-mixed  
270 canopy. This result also supports the assertion that turbulent mixing accounts for the  
271 isoprene removal during the transition period in the STD case. The continuous turbulence in  
272 the STD case is likely sustained by the large-scale forcing (i.e. the relatively high wind speed  
273 above the canopy; Fig. 3d, h). Unlike the STD case, weak turbulence in the EOD case ( $\sigma_w <$   
274  $0.2 \text{ m s}^{-1}$ ) under decoupled conditions is likely generated by local shear instability associated  
275 with nonstationary disturbances, such as density currents, drainage flow, and canopy waves  
276 (Acevedo & Fitzjarrald, 2003; Cava et al., 2004; Alekseychik et al., 2013). Isoprene emissions  
277 at all heights combined with the weak vertical mixing during the decoupling period may  
278 contribute to minimal in-canopy gradients in the EOD case.

279 We use the correlation between the changes in isoprene relative to the peak isoprene  
280 concentration with time ( $\partial[\frac{\text{ISOP}}{\text{ISOP}_{\text{peak}}}] / \partial t$ ) and the standard deviation of the vertical velocity  
281 ( $\sigma_w$ ) to define a critical threshold for  $\sigma_w$  that could inhibit vertical mixing. This threshold  
282 indicates when the emissions dominate over mixing in the late afternoon, and the isoprene  
283 mixing ratio starts to increase. The time period ( $\partial t$ ) used here is the two hours before the  
284 EOD peak for both cases, where isoprene increases in the EOD case and decreases in the STD  
285 case. The peak isoprene concentration ( $\text{ISOP}_{\text{peak}}$ ) is the EOD peak concentration for the  
286 EOD case and the highest isoprene concentration for the STD case (i.e. the concentration at  
287 the beginning of this two-hour period). A critical  $\sigma_w$  of 0.14, 0.2, and  $0.29 \text{ m s}^{-1}$  is identified  
288 for heights of 0.6 z/h (13 m), 0.9 z/h (21 m), and 1.5 z/h (34 m), respectively (Fig. 2e).  
289 In the EOD case,  $\sigma_w$  drop below the critical values and isoprene peaks occur, while in the  
290 STD case  $\sigma_w$  remain above the critical values in the upper canopy (Fig. 2c, d). In the  
291 EOD case, the rate of increase of isoprene shows little correlation with the magnitude of  $\sigma_w$ ,  
292 indicating a negligible contribution of mixing on isoprene mixing ratios. For the STD case,  
293 the rate of change of isoprene is relatively small and becomes less negative with  $\sigma_w$  above  
294 and within the canopy, indicating the varying source strength and/or other sinks (such as  
295 chemical losses) associated with different weather conditions. The results here suggest that a  
296 critical  $\sigma_w$  can be identified to detect the EOD peak in gases with similar or longer chemical  
297 lifetimes as isoprene, and the magnitudes of the critical  $\sigma_w$  depend on the source strength  
298 of the gases such as the daily emission cycle.

### 3.2 Static stability and wind shear

In section 3.1.2, we show a strong relation between low mixing and EOD peak and in section 3.1.1 we hypothesize that clear and calm nights could drive low mixing. Here, we examine the evolution of the stratification and wind shear during the day-to-night transition period (Fig. 3) to provide a mechanistic explanation for the low mixing responsible for the EOD peak and subsequent isoprene removal.

Overall, the virtual potential temperature ( $\theta_v$ ) in the STD case is higher than that in the EOD case. In the STD case, the  $\theta_v$  at the floor of the canopy is 1 Kelvin (K) lower than the canopy top throughout the day-to-night transition period (Fig. 3b), suggesting a weakly stable canopy layer. A weakly stable boundary layer is defined as the regime in which turbulence is continuous and thus the dominant transport process, distinguishable from a very stable boundary layer where turbulence is relatively weak compared to other (sub)mesoscale motions such as waves (Nieuwstadt, 1984; Mahrt, 1999; Steeneveld, 2012). The  $\theta_v$  at the canopy top is 3 K higher than aloft, suggesting a weakly unstable layer above the canopy (Fig. 3b). This is likely caused by the heat storage of the canopy based on the large temperature difference between the STD and the EOD cases. Overall, the averaged temperature gradients are small ( $< 3\text{K}$ ). The day-to-day variations in  $\theta_v$  (as shown by the error bars in figure 3a-b) are generally larger than the vertical gradients. However, we note that only two levels of pressure data (36 m and 6 m) are available for the calculation of the  $\theta_v$  (see section 2.3.1) and as a result, we may be underestimating the  $\theta_v$  gradient. To complement the  $\theta_v$  data set, we also examine the dimensionless stability parameter ( $z/L$ ) that expresses the relative roles of shear and buoyancy in the production of turbulence. Values greater than zero indicate stable conditions while values less than zero indicate unstable conditions. Mahrt (1998) divide the stable boundary layer into three stability regimes as a function of  $z/L$ : (i) weakly stable regime ( $0 < z/L < O(0.1)$ ); (ii) intermediate regime ( $O(0.1) < z/L < O(1)$ ) where the strength of turbulence decreases rapidly with increasing stability; (iii) very stable regime ( $z/L > O(1)$ ). In the STD case, the boundary layer becomes stable after 19:00 LT as  $z/L$  became positive (Fig. 3f). The  $z/L$  is generally less than 0.1, indicating a weakly stable boundary layer. This is in agreement with the results from the  $\theta_v$  profiles described above. In a weakly stable boundary layer, continuous turbulence in the evening can only be sustained by wind shear. The wind speed above the canopy ( $> 2 \text{ m s}^{-1}$  at 36 m and  $> 4 \text{ m s}^{-1}$  at 46 m) is relatively high (Fig. 3d, h) and appears to sustain the continuous turbulence as shown in Figure 2d, suggesting the wind speed here is above the minimum wind speed for sustainable turbulence proposed by (Van de Wiel et al., 2012). In summary, the high wind speed ( $> 4 \text{ m s}^{-1}$  at 46 m) is able to sustain the turbulence in the stable boundary layer during the day-to-night transition period.

335 For the EOD case, a stable boundary layer evolves early in the evening and becomes  
 336 less stable later at night (Fig. 3a, e). Two hours before the EOD peak, even though the  
 337 canopy layer is already stable, the  $\theta_v$  at the canopy top is 2 K higher than in the overlying  
 338 air, suggesting a weakly unstable air layer between  $z/h = 1$  and  $z/h = 1.5$ . As the radiative  
 339 cooling continues, a very stable layer is established over the EOD period (19:30 - 21:30 LT),  
 340 demonstrated by the  $z/L$  values reaching 4. This large  $z/L$  is likely forced by the near-zero  
 341 winds (Fig. 3g) that cause a very small  $L$ . Turbulence production then depends on wind  
 342 shear in the stable boundary layer. Wind speed above the canopy is low ( $<1.5 \text{ m s}^{-1}$ ; Fig.  
 343 3c), suggesting little wind shear production. Even though the wind speed above the canopy  
 344 (46 m) continues to increase during this period (Fig. 3g), the turbulence is still weak as  
 345 shown in section 3.1.2. These results indicate, unlike the STD case, the wind speed above  
 346 the canopy ( $< 3.4 \text{ m s}^{-1}$  at 46 m and  $<1.5 \text{ m s}^{-1}$  at 36 m) is inadequate to sustain the  
 347 turbulence. Therefore, the combination of stratification and weak wind lead to the reduction  
 348 of turbulence during the EOD period (19:30 - 21:30 LT).

349 As the wind increases progressively after the EOD peak (Fig. 3g), the  $z/L$  values drop  
 350 to less than 1 (Fig. 3e), indicating the transition from a very stable canopy layer to a less  
 351 stable canopy layer. Previous studies (Mahrt et al., 2012; Sun et al., 2012; Russell et al.,  
 352 2016) show that there is a threshold point at which stable condition turbulence switches  
 353 from being independent of wind speed to being dependent on wind speed. During the EOD  
 354 period (19:30 - 21:30 LT), the turbulence does not respond to the increase in wind speed.  
 355 However, after the wind speed becomes greater than a certain value ( $> 3.4 \text{ m s}^{-1}$  at 46 m;  
 356 Fig. 3g), the stability is reduced (Fig. 3e) and  $\sigma_w$  above the canopy increases (Fig. 2c).

357 The dependence of  $\sigma_w$  on the mean wind speed is explored to identify the threshold wind  
 358 speed and thus to illustrate the recovery of turbulence in the EOD case (Fig. 4). A clear  
 359 relation between the  $\sigma_w$  and the wind speed exists when the wind speed ( $u$ ) is greater than  
 360  $2.4 \text{ m s}^{-1}$  (Fig. 4). Sun et al. (2012) define a threshold wind speed, after which turbulence  
 361 intensity increases rapidly using the correlation of the turbulence intensity with the mean  
 362 wind speed. According to Sun et al. (2012), the value of  $2.4 \text{ m s}^{-1}$  can be identified as the  
 363 threshold wind speed using Figure 4. In addition, the data suggest a two-term exponential  
 364 form ( $\sigma_w = 0.18e^{-0.17u} + 0.02e^{0.75u}$ ,  $R^2=0.98$ ) with the second term accounting for the  
 365 rapid increase of  $\sigma_w$  at higher wind speeds and both terms explaining the slow increase  
 366 of  $\sigma_w$  at lower wind speeds. We define the wind speed where the second term becomes  
 367 dominant over the sum of the two terms (i.e.  $\frac{\text{term2}}{\text{term1+term2}} > 50\%$ ) as the threshold value.  
 368 This gives a threshold wind speed of  $2.5 \text{ m s}^{-1}$  that is in agreement with the value ( $2.4 \text{ m}$   
 369  $\text{s}^{-1}$ ) identified using Figure 4 as well as previous studies on the stable boundary layer in  
 370 forested environments (e.g. Russell et al. 2016).

371 Turbulence in the stable boundary layer has been categorized into various regimes  
372 based on different governing variables or threshold values (Mahrt, 1999; de Wiel et al.,  
373 2003; Sun et al., 2012). For example, Sun et al. (2012) uses the threshold wind speed to  
374 define turbulent regimes, including (i) regime 1 ( $u < 2.5 \text{ m s}^{-1}$ ), a weak turbulence regime  
375 where the  $\sigma_w$  shows little dependence on the mean wind speed  $u$ ; (ii) regime 2 ( $u > 2.5 \text{ m}$   
376  $\text{s}^{-1}$ ), a strong turbulence regime when the  $\sigma_w$  increases rapidly with  $u$ . The  $\sigma_w$  in regime 1  
377 is predominately from two hours before and at the EOD peaks. These  $\sigma_w$  at the EOD peak  
378 (red symbols in Fig. 4) increase as the wind speed exceeding the threshold value after the  
379 EOD peaks (cyan symbols in Figure 4), suggesting the re-enhancement of turbulence. The  
380  $\sigma_w$  of regime 2 are predominantly from the STD case and the post-peak with two exceptions  
381 (Jul 20 and Jul 28 2016). However, the increases in the  $\sigma_w$  after the EOD peaks in these  
382 two cases still suggest the reinstate of the turbulence by the winds as other EOD cases.  
383 Some of the post-peak  $\sigma_w$  are still below the critical  $\sigma_w$  ( $0.29 \text{ m s}^{-1}$ , Fig. 2e), however,  
384 the critical  $\sigma_w$  is based on changes in isoprene before the peak occurs when emissions are  
385 still occurring. In the post-peak period (21:00-22:00 LT), emissions have likely ceased and  
386 lower  $\sigma_w$  is required to reduce isoprene concentrations. In summary, the wind speed of  $2.5$   
387  $\text{m s}^{-1}$  can be considered as the threshold wind speed where turbulence becomes dependent  
388 on the mean wind speed in this study. For the EOD case, turbulence is reduced due to  
389 stratification and weak wind during the clear and calm nights, leading to the EOD peak  
390 (i.e. accumulation of isoprene in the canopy). However, the wind speed above the canopy  
391 increases to the threshold value after the EOD peak, and turbulence is then reinstated.  
392 The recovery of turbulence produced by wind shear plays an importance role in the rapid  
393 isoprene removal (see section 3.3.1).

### 394 **3.3 Nighttime removal of isoprene**

#### 395 *3.3.1 Contributions of chemistry and vertical mixing to the nighttime re-* 396 *moval*

397 The observed isoprene loss rates from 21:00 LT - 22:00 LT are  $0.57 \text{ hr}^{-1}$  and  $0.55 \text{ hr}^{-1}$   
398 on average for the EOD and STD case, respectively (Fig. 5). The similar magnitude of  
399 the two loss rates suggests that the processes responsible for this rapid decline are similar.  
400 Previous studies also report similar loss rates of isoprene at this study site (Hurst et al., 2001)  
401 as well as in other forested sites (Doughty et al., 2013). Assuming horizontal homogeneity  
402 at the study site, the possible nighttime sinks for isoprene are vertical mixing and chemical  
403 reactions with OH, ozone ( $\text{O}_3$ ), and nitrate radicals ( $\text{NO}_3$ ). No significant dry deposition  
404 of isoprene has been observed to date, probably due to its nonpolar structure (Hurst et

405 al., 2001) and the high surface resistance (Wesely, 2000). In this section, we constrain the  
406 possible loss rates noted above using available observations.

407 Because the in-canopy rapid decay typically initiates between 21:00 PM and 22:00 PM  
408 (referred to as “the decay period” hereinafter), the average concentrations of the oxidants  
409 (OH, O<sub>3</sub>, and NO<sub>3</sub>) over this period are used to calculate the chemical loss rates. The  
410 AMOS 2016 campaign-average OH is  $6.19 \times 10^4 \text{ cm}^{-3}$  for the decay period, resulting in an  
411 average loss rate of  $0.02 \text{ hr}^{-1}$  (Fig. 5). The standard deviation ( $1\sigma$ ) of the measured OH  
412 is  $8.86 \times 10^5 \text{ cm}^{-3}$  and represents the daily variations as well as the precision of the mea-  
413 surements from the top of the tower. The uncertainty associated with the calibration of  
414 the OH instrument is approximately 18% (Dusanter et al., 2008). The PROPHET 1998  
415 (Program for Research on Oxidants: PHotochemistry, Emissions, and Transport) and the  
416 CABINEX 2009 (Community Atmosphere-Biosphere INteractions EXperiment) campaigns  
417 at this study site reported an average nighttime OH concentrations of  $1.1 \times 10^6 \text{ cm}^{-3}$  mea-  
418 sured by the Penn State laser-induced fluorescence (LIF) instrument (Faloona et al., 2001)  
419 and  $3.75 \times 10^5 \text{ cm}^{-3}$  measured by the Indiana University Fluorescence Assay by Gas Ex-  
420 pansion (IU-FAGE) instrument (Griffith et al., 2013), respectively. These concentrations  
421 are approximately 18 and 6 times higher than that measured during AMOS 2016. Recent  
422 studies have noted that unknown interferences may contribute to the reported OH concen-  
423 trations in LIF measurements that only used a wavelength modulation technique without  
424 a chemical removal system (Feiner et al., 2016). This is one possible explanation for the  
425 higher nighttime OH concentrations obtained during the PROPHET 1998 and CABINEX  
426 2009 campaigns. Measurements of potential interferences associated with the IU-FAGE  
427 instrument during CABINEX 2009 suggest that an unknown interference potentially ac-  
428 counts for 50-100 % of the nighttime OH concentrations (Griffith et al., 2013). However, as  
429 discussed above, the chemical removal system used during AMOS 2016 did not reveal any  
430 significant interference, suggesting that the measured concentration during the in-canopy  
431 decay period accurately reflect the ambient OH concentration above the canopy. Given the  
432 low radiation and high isoprene concentrations in the canopy in the early evening, the OH  
433 concentration in the canopy may be even lower than that above the canopy. Therefore, the  
434 observed OH concentrations are inadequate to account for the observed isoprene loss rates  
435 at night at the study site, yet more precise and accurate measurements are needed to reduce  
436 the uncertainties.

437 Reaction of O<sub>3</sub> with isoprene is much slower than with OH. The average O<sub>3</sub> mixing  
438 ratios during the decay period are  $28(\pm 11)$  ppbv and  $20(\pm 9)$  ppbv for the STD and EOD  
439 case, respectively. O<sub>3</sub> measurements were made in the trunk space (6 m) where O<sub>3</sub> concen-  
440 trations are generally lower than those in upper canopy and above canopy especially when

441 vertical mixing is low (Freire et al., 2017). Therefore, the lower O<sub>3</sub> concentrations in the  
442 EOD case provide additional support to the likelihood of low vertical mixing driving the  
443 EOD isoprene peak. Given that the mixing remains relatively high in the STD case, O<sub>3</sub> is  
444 assumed to be well-mixed and represent the concentrations in the upper canopy. Therefore,  
445 the O<sub>3</sub> concentrations in the STD case (28±11 ppbv) were used to calculate the isoprene  
446 loss rate, leading to 5(±2) % of the observed isoprene loss rate for both cases. Note that  
447 this loss rate acts as an upper bound for the EOD case, as the lower mixing would also  
448 reduce O<sub>3</sub> transport into the canopy.

449 NO<sub>3</sub> has been shown to be the main factor for nighttime isoprene decay in high-NO<sub>X</sub>  
450 regions (Brown et al., 2009; Doughty et al., 2013; Millet et al., 2016). An average NO<sub>X</sub>  
451 level of 0.77(±0.73) ppbv and 0.70(±0.62) ppbv were observed during the decay period for  
452 the EOD and STD case respectively, indicating clean conditions at the study site. The  
453 combination of low NO<sub>X</sub> and aforementioned low O<sub>3</sub> levels results in NO<sub>3</sub> mixing ratios  
454 that are always below the limit of detection of the instrument (LOD=1.4 pptv) during the  
455 decay period for both cases. In fact, 93 % of the NO<sub>3</sub> measured during the entire campaign  
456 are below LOD with a maximum of 3.9 pptv. Measurements at other clean forest sites  
457 also show that NO<sub>3</sub> mixing ratios in the canopy are nearly always below a LOD of 1.3–1.4  
458 pptv (Liebmann et al., 2018). If all isoprene loss were attributed to reaction with NO<sub>3</sub>, the  
459 observed isoprene loss rates would require a NO<sub>3</sub> of 10 pptv on average, which would be  
460 an order of magnitude larger than observed. Therefore, NO<sub>3</sub> is not expected to be large  
461 enough to cause the observed isoprene removal at the study site. Because all measurements  
462 are below the LOD, we use the Forest Canopy Atmosphere Transfer model (Ashworth et al.,  
463 2015), as constrained by isoprene, O<sub>3</sub>, NO<sub>X</sub> measurements, to estimate NO<sub>3</sub>. An estimate  
464 of 1.1(±0.05) pptv was obtained, accounting for only 11(±0.5) % of the observed isoprene  
465 loss rates for both cases (Fig. 5). Hurst et al. (2001) estimate a maximum NO<sub>3</sub> of 1.7 pptv  
466 for an NO<sub>2</sub> and O<sub>3</sub> of 1.0 ppbv and 77.1 ppbv during the decay period for the same study  
467 site. Our estimate of NO<sub>3</sub> is slightly lower due to the lower NO<sub>2</sub> and O<sub>3</sub> concentrations  
468 observed.

469 In summary, the chemical losses in total can account for 20 % of the observed isoprene  
470 loss rates for both EOD and STD cases. The largest uncertainty in the chemical loss  
471 estimation described above lies in the dusk-to-nighttime OH concentrations. For example,  
472 if the true OH concentrations during the decay period were higher than the reported values  
473 by an average of 1σ, OH removal could explain up to 60 % of the observed isoprene loss  
474 (Fig. 5).

475 To estimate the isoprene loss rate due to turbulent mixing, we use a residual method.  
476 The residual (LR<sub>mix\_res</sub>) between the observed and the total chemical losses are then con-

477 sidered as the contribution by mixing, accounting for 80 % of the observed loss rates for  
478 both EOD and STD case on average. The estimated loss rate in response to vertical mixing  
479 (LR<sub>mix\_est</sub>) is calculated from the sonic anemometer data using equation 4. This estimate  
480 is similar to the residual for the EOD case (LR<sub>mix\_est</sub> = 0.45 ± 0.21 hr<sup>-1</sup>; LR<sub>mix\_res</sub> =  
481 0.45 hr<sup>-1</sup>) and 30 % higher than the residual for the STD case (LR<sub>mix\_est</sub> = 0.57 ± 0.15  
482 hr<sup>-1</sup>; LR<sub>mix\_res</sub> = 0.44 hr<sup>-1</sup>). Discrepancies between the two estimates (LR<sub>mix\_res</sub> and  
483 LR<sub>mix\_est</sub>) may be attributed to (i) uncertainties in the estimation of LR<sub>mix\_est</sub> associ-  
484 ated with the choice of stable boundary height and the value of [ISOP]<sub>above</sub>/[ISOP]<sub>in-canopy</sub>  
485 (Section 2.3); (ii) and/or the lack of interactions between physical and chemical processes in  
486 LR<sub>mix\_res</sub> which could be important under stable/nighttime conditions (Freire et al., 2017).  
487 For example, incomplete mixing could cause segregation between isoprene and OH and thus  
488 reduction in the reaction rates (Kim et al., 2016), which would lead to a lower chemical loss  
489 rate and then a higher residual loss rate due to mixing. Overall, the LR<sub>mix\_est</sub> agree with  
490 LR<sub>mix\_res</sub>. Note that the similarity of the loss rates between the EOD and STD cases  
491 (Fig. 5) suggests that the main process responsible for this rapid decline are similar (i.e.  
492 turbulent mixing). This is supported by the sustained turbulence by the continuously high  
493 wind speeds in the STD case, and by the reintroduction of turbulent mixing by increased  
494 winds above the canopy in the EOD case.

495 Further evidence of turbulent mixing accounting for the observed isoprene loss rates  
496 could be supported by positive isoprene fluxes above the canopy during the decay period.  
497 However, the isoprene flux data are not valid because of low turbulence (the friction velocity  
498  $u_* < 0.2 \text{ m s}^{-1}$ ) during the decay period for the EOD case. For the STD case, the average  
499 isoprene flux ( $F_{\text{OBS}}$ ) during the decay period is 0.01(±0.01) ppbv m s<sup>-1</sup>. To establish a  
500 metric to explain and assess the magnitude of the observed flux, a flux-gradient method  
501 (i.e.  $F_{\text{Cal}} = -K \frac{\Delta C}{\Delta z}$ ) was used to estimate the isoprene fluxes. The calculation suggests  
502 an average of 0.18 ppbv m s<sup>-1</sup> and 0.03 ppbv m s<sup>-1</sup> for  $F_{\text{Cal}}$  for the EOD and STD case,  
503 respectively. The estimated and measured isoprene fluxes are in the same order of magnitude  
504 for the STD case, serving as a verification of the fidelity of the flux-gradient method for the  
505 decay period. From flux-gradient theory, it is reasonable to suppose a higher isoprene flux in  
506 the EOD case given the greater concentration gradient ( $\Delta C_{\text{EOD}} = -3.84$  ppbv,  $\Delta C_{\text{STD}} = -0.42$   
507 ppbv) but similar eddy diffusivity ( $K_{\text{EOD}} = 0.62 \text{ m}^2 \text{ s}^{-1}$ ,  $K_{\text{STD}} = 0.89 \text{ m}^2 \text{ s}^{-1}$ ). However, the  
508 observations did not capture the fluxes corresponding to the removal of the accumulated  
509 isoprene for the EOD case. There are several possible reasons for this discrepancy. First,  
510 the majority of the isoprene fluxes associated with the EOD peak might not be captured  
511 by the flux measurements measured 30 minutes later due to the time differences between  
512 the gradient and flux observations (see Section 2.3). Second, eddies associated with the  
513 weak turbulence transporting isoprene out of the canopy during the decay period in the



514 EOD case might be too small to be captured by the eddy covariance system placed at 10 m  
515 above the canopy. The calculation-observation discrepancy also raises a possibility that the  
516 assumption of horizontal homogeneity used here is invalid for the EOD case at the study  
517 site (see discussion in Section 3.3.2).

### 518 *3.3.2 Influences of advection on the nighttime removal*

519 Section 3.2 described the observed increased wind speed to a critical value and its effect  
520 of increasing the turbulent mixing in the EOD case, indicating that synoptic forcing becomes  
521 important in the stable boundary layer. In this study, a wind direction shift from the north  
522 to the south was observed along with the increase in wind speed for 85 % of the EOD peak  
523 events (e.g. Fig. 1f). Because this wind direction shift occurs after the isoprene peak,  
524 we hypothesize that horizontal advection is an important driver of the nighttime isoprene  
525 decline. This shift in wind direction resembles lake breeze that has been observed in the  
526 Great Lake regions (Moroz, 1967). The lake breeze is most frequently observed in July and  
527 August due to the minimal daytime cloudiness and the low wind speeds that maximize the  
528 land-lake temperature differences in the Great Lake regions (Ryznar & Touma, 1981). Note  
529 that the clear and calm conditions during which the EOD peak developed also favor the  
530 lake breezes by enhancing the land-lake temperature differences.

531 The lake breeze phenomenon would introduce another uncertainty (i.e. advection) in  
532 the investigation of nighttime isoprene removal. Assuming horizontal homogeneity (i.e. no  
533 advection) for simplicity and analytical tractability, we show the rapid removal of isoprene  
534 could be driven by vertical mixing for the EOD case (Section 3.3.1). However, Sun et al.  
535 (1998) showed that a lake breeze could generate a significant advection for CO<sub>2</sub>. If this is the  
536 case for isoprene, the small fluxes measured above the canopy as well as the rapid isoprene  
537 removal could be due to the significant advection dominating over the vertical mixing. This  
538 hypothesis of advection is supported by the increased wind and the wind direction shift  
539 (Fig. 1e, f and Fig. 3c, g). The advection can be estimated by vertical flux divergence  
540 measurements made on very tall towers (Lee & Hu, 2002), yet these measurements do not  
541 exist at the site. More data are required to validate the occurrence of lake breeze and  
542 quantify the contribution of advection in the nighttime isoprene removal.

## 543 **4 Summary and Conclusions**

544 Seven days (23 % of the measurement period) during the 2016 AMOS field campaign  
545 are identified as having an end-of-day peak in isoprene mixing ratio. The peak occurs around  
546 sunset (21:30 local time) and the in-canopy isoprene increases by 77 % (from 3.5 ppbv to  
547 6.2 ppbv) on average. Stratification and weak wind ( $< 3.4 \text{ m s}^{-1}$  at 46 m) during clear

548 and calm nights significantly suppress turbulent exchanges between in- and above-canopy,  
549 leading to the accumulation of isoprene emitted at dusk in the canopy, observed as the EOD  
550 peak. A critical  $\sigma_w$  of 0.14, 0.2, and 0.29 m s<sup>-1</sup> is identified to detect the EOD peak for  
551 the height of 13, 21, and 34 m, respectively. As wind speeds increases, mixing recovers to  
552 reduce isoprene mixing ratios. Observed shifts in wind direction suggests that the increased  
553 wind speed could be attributed to the lake breezes. When the wind speed increased above  
554 2.5 m s<sup>-1</sup>, turbulence is enhanced again. Therefore, a wind speed of 2.5 m s<sup>-1</sup> is considered  
555 as the threshold point where turbulence switches from being independent of wind speed to  
556 dependent on wind speed. However, in the standard case where wind speed is greater than  
557 the threshold point throughout the evening hours, turbulence is sustained ( $\sigma_w > 0.4$  m s<sup>-1</sup>)  
558 by wind shear and no EOD peak is observed.

559 The observed isoprene exhibit similar loss rates for the EOD and standard cases of  
560 0.57 hr<sup>-1</sup> and 0.55 hr<sup>-1</sup> on average, respectively. Measured OH, O<sub>3</sub>, and NO<sub>3</sub> suggest that  
561 chemical losses in total accounts for 20% of the observed loss rate for both cases. The largest  
562 uncertainty in the chemical loss estimation is associated with the OH instrument. Estimated  
563 turbulent mixing timescales suggest that turbulent mixing accounts for the remaining 80%  
564 of the observed loss rates. Observations did not capture the fluxes corresponding to the  
565 turbulent removal of the accumulated isoprene in the canopy, and this may be due to the  
566 sampling intervals used to quantify both fluxes and concentration gradients or challenges  
567 in micrometeorological methods under stable conditions. Another possible reason is that  
568 advection induced by the lake-breeze-like motion dominates over the vertical mixing, indi-  
569 cating the assumption of horizontal homogeneity may not be valid under calm and clear  
570 nighttime conditions at the study site. However, measurements do not exist at the site to  
571 test this hypothesis.

572 In summary, stagnant days characterized with clear and calm conditions promote the  
573 cooling of the canopy and thus low mixing conditions that lead to the EOD peak. These  
574 stagnant conditions are unable to sustain the isoprene peak for more than 2 hours due  
575 to enhanced wind speed generated by the developments of a lake-breeze-like motion in  
576 the atmosphere. This interesting behavior of isoprene has been reported in many forested  
577 regions, but none of previous work provided a clear explanation that accounts for both  
578 physical and chemical processes. This study presents representative atmospheric dynamics  
579 and chemistry data for temperate forest sites and discuss the possible mechanisms, providing  
580 a frame of reference for understanding in-canopy behaviors of reactive gases in forested  
581 environments. In addition, these results highlight unique features about reactive in-canopy  
582 chemistry. Models are known to have difficulties capturing transitions in the boundary layer

583 from dawn to dusk, and this study illuminates the processes of isoprene in the canopy and  
584 its transfer to the free troposphere.

Author Manuscript

**Acknowledgments**

We acknowledge support by National Oceanic and Atmospheric Administration under grant NA18OAR4310116. DBM and HDA acknowledge support from the National Science Foundation (grants 1932771 and 1428257). ML, BB, and PS acknowledge grants from the National Science Foundation (AGS-1440834 and AGS-1827450). Data are available through Alwe et al. (2019).

**References**

- Acevedo, O. C., & Fitzjarrald, D. R. (2003). In the core of the night-effects of intermittent mixing on a horizontally heterogeneous surface. *Boundary-Layer Meteorology*, *106*(1), 1–33. doi: 10.1023/A:1020824109575
- Alekseychik, P., Mammarella, I., Launiainen, S., Rannik, ., & Vesala, T. (2013). Evolution of the nocturnal decoupled layer in a pine forest canopy. *Agricultural and Forest Meteorology*, *174-175*, 15–27. doi: 10.1016/j.agrformet.2013.01.011
- Alwe, H. D., Millet, D. B., Chen, X., Raff, J. D., Payne, Z. C., & Fledderman, K. (2019). Oxidation of volatile organic compounds as the major source of formic acid in a mixed forest canopy. *Geophysical Research Letters*, *46*(5), 2940–2948. doi: 10.1029/2018GL081526
- Apel, E. C. (2002). Measurement and interpretation of isoprene fluxes and isoprene, methacrolein, and methyl vinyl ketone mixing ratios at the PROPHET site during the 1998 intensive. *Journal of Geophysical Research*, *107*(D3). doi: 10.1029/2000JD000225
- Ashworth, K., Chung, S. H., Griffin, R. J., Chen, J., Forkel, R., Bryan, A. M., & Steiner, A. L. (2015). FORest canopy atmosphere transfer (FORCAsT) 1.0: a 1-d model of biosphere–atmosphere chemical exchange. *Geoscientific Model Development*, *8*(11), 3765–3784. doi: 10.5194/gmd-8-3765-2015
- Brown, S. S., deGouw, J. A., Warneke, C., Ryerson, T. B., Dubé, W. P., Atlas, E., . . . Ravishankara, A. R. (2009). Nocturnal isoprene oxidation over the northeast united states in summer and its impact on reactive nitrogen partitioning and secondary organic aerosol. *Atmospheric Chemistry and Physics*, *9*(9), 3027–3042. doi: 10.5194/acp-9-3027-2009
- Burns, S. P., Sun, J., Lenschow, D. H., Oncley, S. P., Stephens, B. B., Yi, C., . . . Monson, R. K. (2010). Atmospheric stability effects on wind fields and scalar mixing within and just above a subalpine forest in sloping terrain. *Boundary-Layer Meteorology*, *138*(2), 231–262. doi: 10.1007/s10546-010-9560-6
- Cava, D., Giostra, U., Siqueira, M., & Katul, G. (2004). Organised motion and radiative perturbations in the nocturnal canopy sublayer above an even-aged pine forest. *Boundary-Layer Meteorology*, *112*(1), 129–157. doi: 10.1023/B:BOUN.0000020160.28184.a0
- Claeys, M. (2004, feb). Formation of secondary organic aerosols through photooxidation of

- isoprene. *Science*, *303*(5661), 1173–1176. doi: 10.1126/science.1092805
- Cooper, O. R., Moody, J. L., Thornberry, T. D., Town, M. S., & Carroll, M. A. (2001, oct). PROPHET 1998 meteorological overview and air-mass classification. *Journal of Geophysical Research: Atmospheres*, *106*(D20), 24289–24299. doi: 10.1029/2000JD900409
- de Arellano, J. V.-G., Patton, E. G., Karl, T., van den Dries, K., Barth, M. C., & Orlando, J. J. (2011). The role of boundary layer dynamics on the diurnal evolution of isoprene and the hydroxyl radical over tropical forests. *Journal of Geophysical Research*, *116*(D7). doi: 10.1029/2010JD014857
- de Wiel, B. J. H. V., Moene, A. F., Hartogensis, O. K., Bruin, H. A. R. D., & Holtslag, A. A. M. (2003, oct). Intermittent turbulence in the stable boundary layer over land. part III: A classification for observations during CASES-99. *Journal of the Atmospheric Sciences*, *60*(20), 2509–2522. doi: 10.1175/1520-0469(2003)060<2509:ITITSB>2.0.CO;2
- Doughty, D., Fuentes, J. D., Sakai, R., Hu, X.-M., & Sanchez, K. (2013). Nocturnal isoprene declines in a semi-urban environment. *Journal of Atmospheric Chemistry*, *72*(3-4), 215–234. doi: 10.1007/s10874-012-9247-0
- Dusanter, S., Vimal, D., & Stevens, P. S. (2008). Technical note: Measuring tropospheric OH and HO<sub>2</sub> by laser-induced fluorescence at low pressure: A comparison of calibration techniques. *Atmospheric Chemistry and Physics*, *8*(2), 321–340. doi: 10.5194/acp-8-321-2008
- Dusanter, S., Vimal, D., Stevens, P. S., Volkamer, R., & Molina, L. T. (2009). Measurements of OH and HO<sub>2</sub> concentrations during the MCMA-2006 field campaign – part 1: Deployment of the indiana university laser-induced fluorescence instrument. *Atmospheric Chemistry and Physics*, *9*(5), 1665–1685. doi: 10.5194/acp-9-1665-2009
- Faloona, I., Tan, D., Brune, W., Hurst, J., Barket, D., Couch, T. L., ... Paterson, K. (2001). Nighttime observations of anomalously high levels of hydroxyl radicals above a deciduous forest canopy. *Journal of Geophysical Research: Atmospheres*, *106*(D20), 24315–24333. doi: 10.1029/2000JD900691
- Feiner, P. A., Brune, W. H., Miller, D. O., Zhang, L., Cohen, R. C., Romer, P. S., ... Fry, J. L. (2016). Testing atmospheric oxidation in an alabama forest. *Journal of the Atmospheric Sciences*, *73*(12), 4699–4710. doi: 10.1175/JAS-D-16-0044.1
- Freire, L. S., Gerken, T., Ruiz-Plancarte, J., Wei, D., Fuentes, J. D., Katul, G. G., ... Chamecki, M. (2017). Turbulent mixing and removal of ozone within an amazon rainforest canopy. *Journal of Geophysical Research: Atmospheres*, *122*(5), 2791–2811. doi: 10.1002/2016JD026009
- Fuchs, H., Hofzumahaus, A., Rohrer, F., Bohn, B., Brauers, T., Dorn, H.-P., ... Wahner, A. (2013, oct). Experimental evidence for efficient hydroxyl radical regeneration in isoprene oxidation. *Nature Geoscience*, *6*(12), 1023–1026. doi: 10.1038/ngeo1964

- 657 Goldan, P. D., Kuster, W. C., Fehsenfeld, F. C., & Montzka, S. A. (1995). Hydrocarbon  
658 measurements in the southeastern united states: The rural oxidants in the southern envi-  
659 ronment (ROSE) program 1990. *Journal of Geophysical Research*, *100*(D12), 25945. doi:  
660 10.1029/95JD02607
- 661 Griffith, S. M., Hansen, R. F., Dusanter, S., Michoud, V., Gilman, J. B., Kuster, W. C.,  
662 ... Stevens, P. S. (2016). Measurements of hydroxyl and hydroperoxy radicals during  
663 CalNex-LA: Model comparisons and radical budgets. *Journal of Geophysical Research:  
664 Atmospheres*, *121*(8), 4211–4232. doi: 10.1002/2015JD024358
- 665 Griffith, S. M., Hansen, R. F., Dusanter, S., Stevens, P. S., Alaghmand, M., Bertman,  
666 S. B., ... Zhou, X. L. (2013). OH and HO<sub>2</sub> radical chemistry during PROPHET 2008 and  
667 CABINEX 2009 – part 1: Measurements and model comparison. *Atmospheric Chemistry  
668 and Physics*, *13*(11), 5403–5423. doi: 10.5194/acp-13-5403-2013
- 669 Guenther, A. B., Jiang, X., Heald, C. L., Sakulyanontvittaya, T., Duhl, T., Emmons, L. K.,  
670 & Wang, X. (2012, nov). The model of emissions of gases and aerosols from nature version  
671 2.1 (MEGAN2.1): an extended and updated framework for modeling biogenic emissions.  
672 *Geoscientific Model Development*, *5*(6), 1471–1492. doi: 10.5194/gmd-5-1471-2012
- 673 Guenther, A. B., Zimmerman, P. R., Harley, P. C., Monson, R. K., & Fall, R. (1993).  
674 Isoprene and monoterpene emission rate variability: Model evaluations and sensitivity  
675 analyses. *Journal of Geophysical Research*, *98*(D7), 12609. doi: 10.1029/93JD00527
- 676 Gunch, M. J., May, N. W., Wen, M., Bottenus, C. L. H., Gardner, D. J., VanReken, T. M.,  
677 ... Pratt, K. A. (2018, mar). Ubiquitous influence of wildfire emissions and secondary  
678 organic aerosol on summertime atmospheric aerosol in the forested great lakes region.  
679 *Atmospheric Chemistry and Physics*, *18*(5), 3701–3715. doi: 10.5194/acp-18-3701-2018
- 680 Hurst, J. M., Barket, D. J., Herrera-Gomez, O., Couch, T. L., Shepson, P. B., Faloon, I., ...  
681 Carroll, M. A. (2001). Investigation of the nighttime decay of isoprene. *Journal of Geo-  
682 physical Research: Atmospheres*, *106*(D20), 24335–24346. doi: 10.1029/2000JD900727
- 683 Kim, S.-W., Barth, M. C., & Trainer, M. (2016, jul). Impact of turbulent mixing on isoprene  
684 chemistry. *Geophysical Research Letters*, *43*(14), 7701–7708. doi: 10.1002/2016gl069752
- 685 Lee, X., & Hu, X. (2002, may). Forest-air fluxes of carbon, water and energy over non-flat  
686 terrain. *Boundary-Layer Meteorology*, *103*(2), 277–301. doi: 10.1023/A:1014508928693
- 687 Lelieveld, J., Butler, T. M., Crowley, J. N., Dillon, T. J., Fischer, H., Ganzeveld, L., ...  
688 Williams, J. (2008). Atmospheric oxidation capacity sustained by a tropical forest. *Nature*,  
689 *452*(7188), 737–740. doi: 10.1038/nature06870
- 690 Levy, H. (1971). Normal atmosphere: Large radical and formaldehyde concentrations  
691 predicted. *Science*, *173*(3992), 141–143. doi: 10.1126/science.173.3992.141
- 692 Liang, J., Zhang, L., Wang, Y., Cao, X., Zhang, Q., Wang, H., & Zhang, B. (2014, may).

- 693 Turbulence regimes and the validity of similarity theory in the stable boundary layer  
694 over complex terrain of the loess plateau, china. *Journal of Geophysical Research: Atmo-*  
695 *spheres*, 119(10), 6009–6021. doi: 10.1002/2014JD021510
- 696 Liebmann, J., Karu, E., Sobanski, N., Schuladen, J., Ehn, M., Schallhart, S., . . . Crowley,  
697 J. N. (2018). Direct measurement of NO<sub>3</sub> radical reactivity in a boreal forest. *Atmospheric*  
698 *Chemistry and Physics*, 18(5), 3799–3815. doi: 10.5194/acp-18-3799-2018
- 699 Liu, C.-M. (2008). Complete solutions to extended stokes' problems. *Mathematical Problems*  
700 *in Engineering*, 2008, 1–18. doi: 10.1155/2008/754262
- 701 Mahrt, L. (1998, aug). Nocturnal boundary-layer regimes. *Boundary-Layer Meteorology*,  
702 88(2), 255–278. doi: 10.1023/A:1001171313493
- 703 Mahrt, L. (1999). Stratified atmospheric boundary layers. *Boundary-Layer Meteorology*,  
704 90(3), 375–396. doi: 10.1023/A:1001765727956
- 705 Mahrt, L., Richardson, S., Seaman, N., & Stauffer, D. (2012). Turbulence in the nocturnal  
706 boundary layer with light and variable winds. *Quarterly Journal of the Royal Meteorolo-*  
707 *gical Society*, 138(667), 1430–1439. doi: 10.1002/qj.1884
- 708 Martin, R. S., Westberg, H., Allwine, E., Ashman, L., Farmer, J. C., & Lamb, B. (1991,  
709 jul). Measurement of isoprene and its atmospheric oxidation products in a central  
710 pennsylvania deciduous forest. *Journal of Atmospheric Chemistry*, 13(1), 1–32. doi:  
711 10.1007/BF00048098
- 712 Millet, D. B., Alwe, H. D., Chen, X., Deventer, M. J., Griffis, T. J., Holzinger, R., . . .  
713 Flynn, J. H. (2018, jun). Bidirectional ecosystem–atmosphere fluxes of volatile organic  
714 compounds across the mass spectrum: How many matter? *ACS Earth and Space Chem-*  
715 *istry*, 2(8), 764–777. doi: 10.1021/acsearthspacechem.8b00061
- 716 Millet, D. B., Baasandorj, M., Hu, L., Mitroo, D., Turner, J., & Williams, B. J. (2016).  
717 Nighttime chemistry and morning isoprene can drive urban ozone downwind of a major  
718 deciduous forest. *Environmental Science & Technology*, 50(8), 4335–4342. doi: 10.1021/  
719 acs.est.5b06367
- 720 Montzka, S. A., Trainer, M., Goldan, P. D., Kuster, W. C., & Fehsenfeld, F. C. (1993).  
721 Isoprene and its oxidation products, methyl vinyl ketone and methacrolein, in the rural  
722 troposphere. *Journal of Geophysical Research: Atmospheres*, 98(D1), 1101–1111. doi:  
723 10.1029/92JD02382
- 724 Moroz, W. J. (1967, jul). A lake breeze on the eastern shore of lake michigan: Observations  
725 and model. *Journal of the Atmospheric Sciences*, 24(4), 337–355. doi: 10.1175/1520  
726 -0469(1967)024<0337:ALBOTE>2.0.CO;2
- 727 Ng, N. L., Kwan, A. J., Surratt, J. D., Chan, A. W. H., Chhabra, P. S., Sorooshian, A.,  
728 . . . Seinfeld, J. H. (2008, aug). Secondary organic aerosol (SOA) formation from reaction

- 729 of isoprene with nitrate radicals (NO<sub>3</sub>). *Atmospheric Chemistry and Physics*, 8(14),  
730 4117–4140. doi: 10.5194/acp-8-4117-2008
- 731 Nieuwstadt, F. T. M. (1984, jul). The turbulent structure of the stable, noctur-  
732 nal boundary layer. *Journal of the Atmospheric Sciences*, 41(14), 2202–2216. doi:  
733 10.1175/1520-0469(1984)041<2202:TTSOTS>2.0.CO;2
- 734 Oliveira, P. E. S., Acevedo, O. C., Moraes, O. L. L., Zimmermann, H. R., & Teichrieb, C.  
735 (2012). Nocturnal intermittent coupling between the interior of a pine forest and the air  
736 above it. *Boundary-Layer Meteorology*, 146(1), 45–64. doi: 10.1007/s10546-012-9756-z
- 737 Rebmann, C., Kolle, O., Heinesch, B., Queck, R., Ibrom, A., & Aubinet, M. (2011). *Data*  
738 *acquisition and flux calculations*. Springer Netherlands. doi: 10.1007/978-94-007-2351-1  
739 \_3
- 740 Rickly, P., & Stevens, P. S. (2018). Measurements of a potential interference with laser-  
741 induced fluorescence measurements of ambient OH from the ozonolysis of biogenic alkenes.  
742 *Atmospheric Measurement Techniques*, 11(1), 1–16. doi: 10.5194/amt-11-1-2018
- 743 Robinson, N. H., Hamilton, J. F., Allan, J. D., Langford, B., Oram, D. E., Chen, Q., ...  
744 Coe, H. (2011, feb). Evidence for a significant proportion of secondary organic aerosol  
745 from isoprene above a maritime tropical forest. *Atmospheric Chemistry and Physics*,  
746 11(3), 1039–1050. doi: 10.5194/acp-11-1039-2011
- 747 Russell, E. S., Liu, H., Gao, Z., Lamb, B., & Wagenbrenner, N. (2016). Turbulence  
748 dependence on winds and stability in a weak-wind canopy sublayer over complex ter-  
749 rain. *Journal of Geophysical Research: Atmospheres*, 121(19), 11,502–11,515. doi:  
750 10.1002/2016JD025057
- 751 Ryznar, E., & Touma, J. S. (1981, jan). Characteristics of true lake breezes along the  
752 eastern shore of lake michigan. *Atmospheric Environment (1967)*, 15(7), 1201–1205. doi:  
753 10.1016/0004-6981(81)90311-5
- 754 Sillman, S., Carroll, M. A., Thornberry, T., Lamb, B. K., Westberg, H., Brune, W. H., ...  
755 Zika, R. G. (2002). Loss of isoprene and sources of nighttime OH radicals at a rural site in  
756 the united states: Results from photochemical models. *Journal of Geophysical Research:*  
757 *Atmospheres*, 107(D5), ACH 2–1–ACH 2–14. doi: 10.1029/2001JD000449
- 758 Starn, T. K., Shepson, P. B., Bertman, S. B., Riemer, D. D., Zika, R. G., & Olszyna,  
759 K. (1998). Nighttime isoprene chemistry at an urban-impacted forest site. *Journal of*  
760 *Geophysical Research: Atmospheres*, 103(D17), 22437–22447. doi: 10.1029/98jd01201
- 761 Steeneveld, G. (2012). Stable boundary layer issues. *ECMWF/GABLS Workshop on*  
762 *Diurnal Cycles and the Stable Atmospheric Boundary Layer*, 25–36.
- 763 Sun, J., Desjardins, R., Mahrt, L., & MacPherson, I. (1998, oct). Transport of carbon diox-  
764 ide, water vapor, and ozone by turbulence and local circulations. *Journal of Geophysical*



- 765 *Research: Atmospheres*, 103(D20), 25873–25885. doi: 10.1029/98JD02439
- 766 Sun, J., Mahrt, L., Banta, R. M., & Pichugina, Y. L. (2012). Turbulence regimes and  
767 turbulence intermittency in the stable boundary layer during CASES-99. *Journal of the*  
768 *Atmospheric Sciences*, 69(1), 338–351. doi: 10.1175/JAS-D-11-082.1
- 769 Taraborrelli, D., Lawrence, M. G., Crowley, J. N., Dillon, T. J., Gromov, S., Groß, C. B. M.,  
770 . . . Lelieveld, J. (2012, feb). Hydroxyl radical buffered by isoprene oxidation over tropical  
771 forests. *Nature Geoscience*, 5(3), 190–193. doi: 10.1038/ngeo1405
- 772 Van de Wiel, Moene, A. F., Jonker, H. J. J., Baas, P., Basu, S., Donda, J. M. M., . . .  
773 Holtslag, A. A. M. (2012). The minimum wind speed for sustainable turbulence in the  
774 nocturnal boundary layer. *Journal of the Atmospheric Sciences*, 69(11), 3116–3127. doi:  
775 10.1175/JAS-D-12-0107.1
- 776 Van de Wiel, B., Moene, A. F., & Jonker, H. (2012). The cessation of continuous turbulence  
777 as precursor of the very stable nocturnal boundary layer. *Journal of the Atmospheric*  
778 *Sciences*, 69(11), 3097–3115. doi: 10.1175/JAS-D-12-064.1
- 779 van Gorsel, E., Harman, I. N., Finnigan, J. J., & Leuning, R. (2011). Decoupling of air flow  
780 above and in plant canopies and gravity waves affect micrometeorological estimates of  
781 net scalar exchange. *Agricultural and Forest Meteorology*, 151(7), 927–933. doi: 10.1016/  
782 j.agrformet.2011.02.012
- 783 VanReken, T., Mwaniki, G., Wallace, H., Pressley, S., Erickson, M., Jobson, B., & Lamb,  
784 B. (2015, apr). Influence of air mass origin on aerosol properties at a remote michigan  
785 forest site. *Atmospheric Environment*, 107, 35–43. doi: 10.1016/j.atmosenv.2015.02.027
- 786 Wei, D., Fuentes, J. D., Gerken, T., Chamecki, M., Trowbridge, A. M., Stoy, P. C., . . . dos  
787 Santos, R. M. N. (2018). Environmental and biological controls on seasonal patterns of  
788 isoprene above a rain forest in central amazonia. *Agricultural and Forest Meteorology*,  
789 256-257, 391–406. doi: 10.1016/j.agrformet.2018.03.024
- 790 Wesely, M. (2000). A review of the current status of knowledge on dry deposition. *Atmo-*  
791 *spheric Environment*, 34(12-14), 2261–2282. doi: 10.1016/S1352-2310(99)00467-7

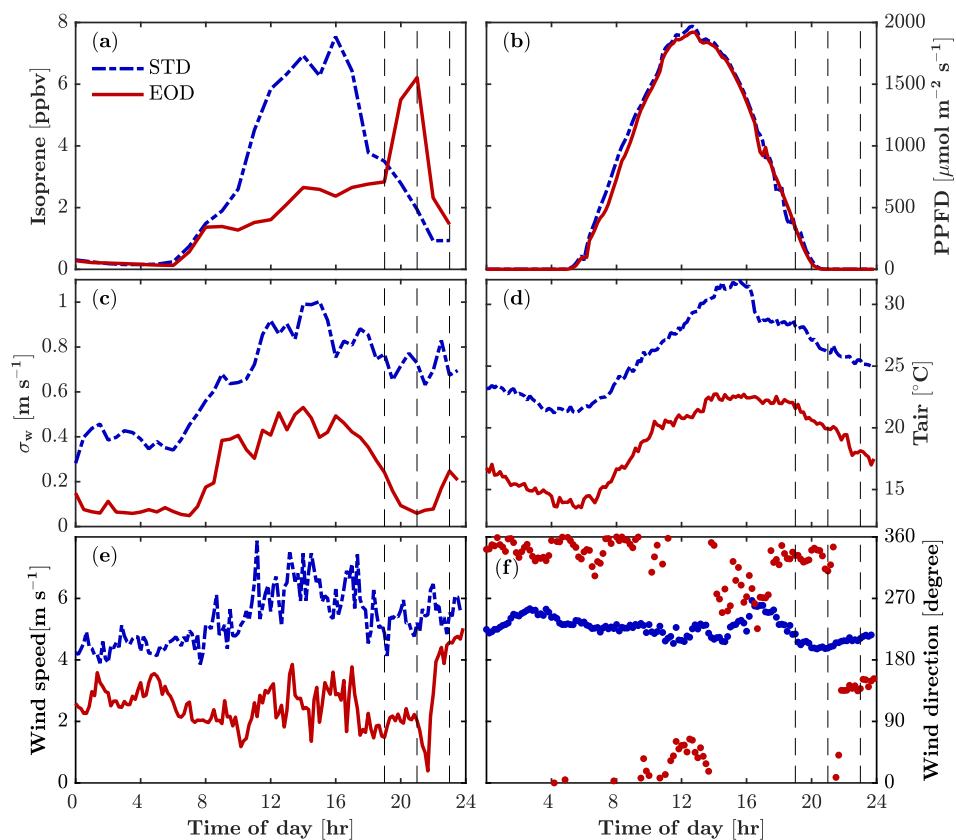


**Figure 1.** Examples of the End-Of-Day peak case (EOD; July 19 2016) and the standard case (STD; July 13 2016). **(a)** Diurnal variations of hourly isoprene mixing ratios [ppbv] at 21 m. **(b)** Diurnal variations of 10-min Photosynthetic Photon Flux Density (PPFD) at 46 m. **(c)** Diurnal variations in half hourly standard deviation of vertical velocity ( $\sigma_w$ ) at 21 m. **(d)** Diurnal variations in 10-min air temperature at 46 m. **(e)** Diurnal variations in hourly isoprene flux at 34 m. **(f)** Diurnal variations in 10-min wind speed (line) and wind direction (dot) at 46 m. **(g, h)** Diurnal variations in 5-min  $\text{NO}_X$  and  $\text{O}_3$  mixing ratios at 6 m, respectively. The canopy height is about 22.5 m.

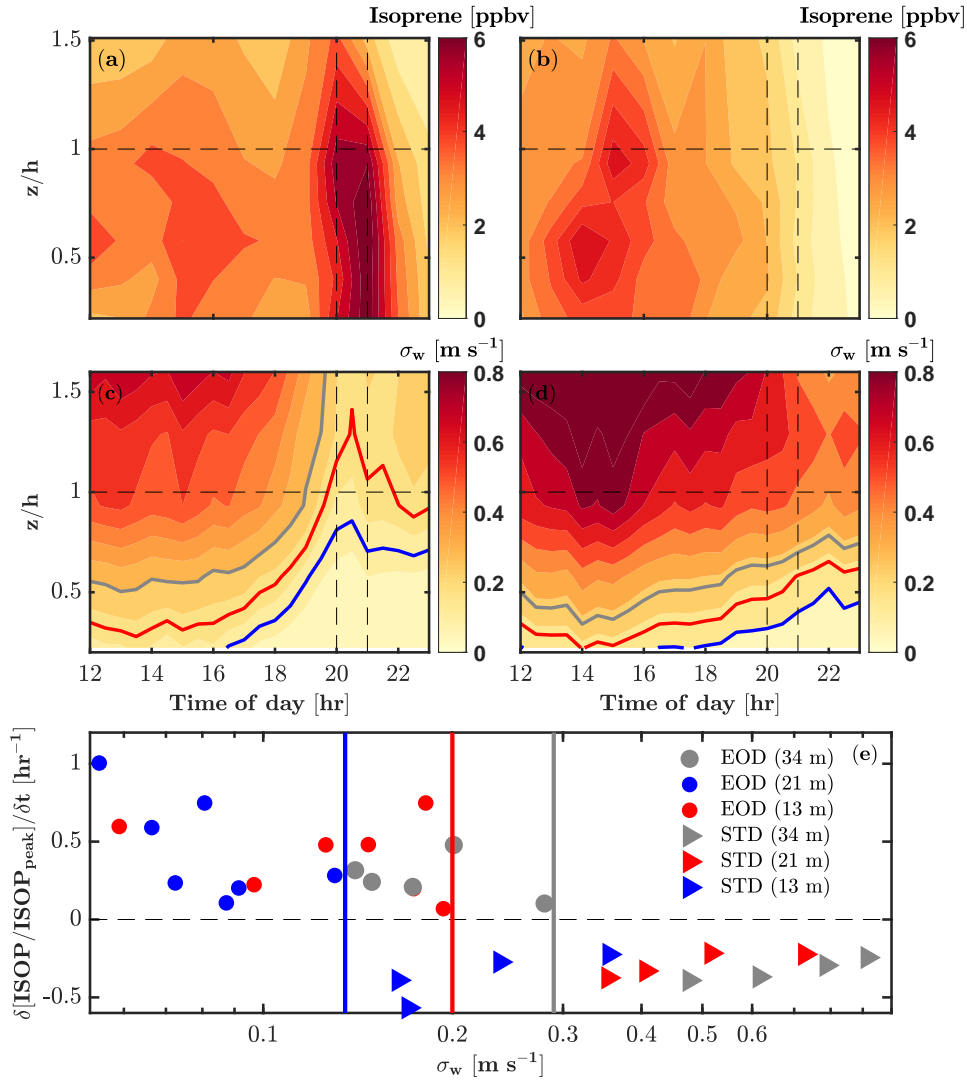


**Figure 2.** In-canopy profiles of isoprene and  $\sigma_w$  averaged over all EOD (a, c) and STD (b, d) cases. Isoprene mixing ratios as a function of local time and height for the EOD case (a) and STD case (b). Averaged  $\sigma_w$  as a function of local time and height for the EOD case (c) and STD case (d). The vertical dashed lines in panels a-d denote the period within 1 hour before the peak (20:00-21:00 local time). The correlation between the changes in isoprene relative to the peak isoprene concentration with time ( $\partial[\frac{\text{ISOP}_{\text{peak}}}{\text{ISOP}_{\text{peak}}}] / \partial t$ ) and  $\sigma_w$  at heights above the canopy (34 m: grey markers) and in the canopy (21 m: red markers; 13 m: blue markers)(e). Data shown in (e) are prior-peak data only. Critical  $\sigma_w$  values are noted with vertical lines for the 3 heights for the EOD cases (circles) and the STD cases (triangles). The contour lines for the critical  $\sigma_w$  values are

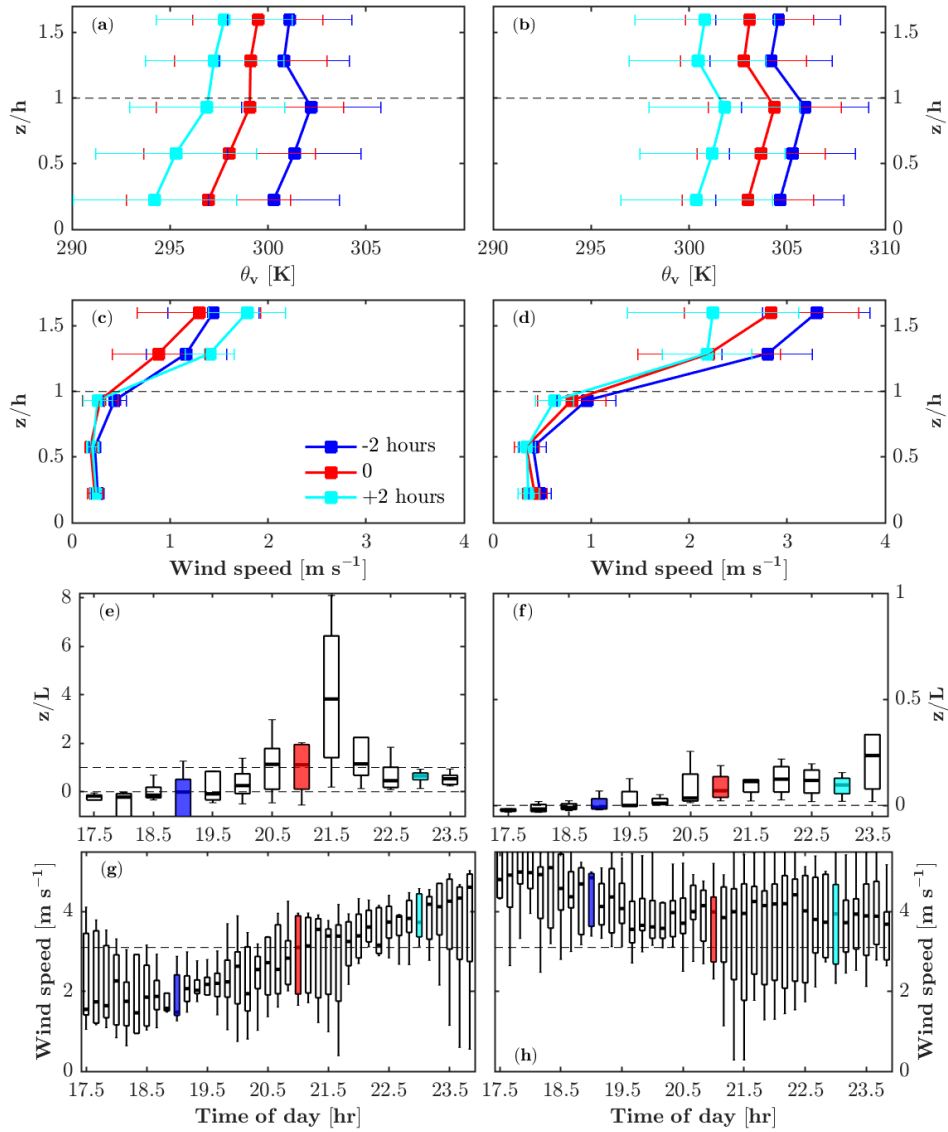


**Figure 3.** Averaged profiles of virtual potential temperature ( $\theta_v$ ) for the EOD case (a) and STD case (b) for these periods: 2 hours before the peak (blue), the average peak time 21:00 LT (red), and 2 hours after the peak (cyan). Averaged profiles of wind speed from sonic anemometers for the EOD case (c) and STD case (d). The evolution of dimensionless stability parameter  $z/L$  for the EOD case (e) and STD case (f) (note different y-axis scales for e and f; a dashed line on e compares the maximum for f). The evolution of wind speed at 46 m for the EOD case (g) and STD case (h).

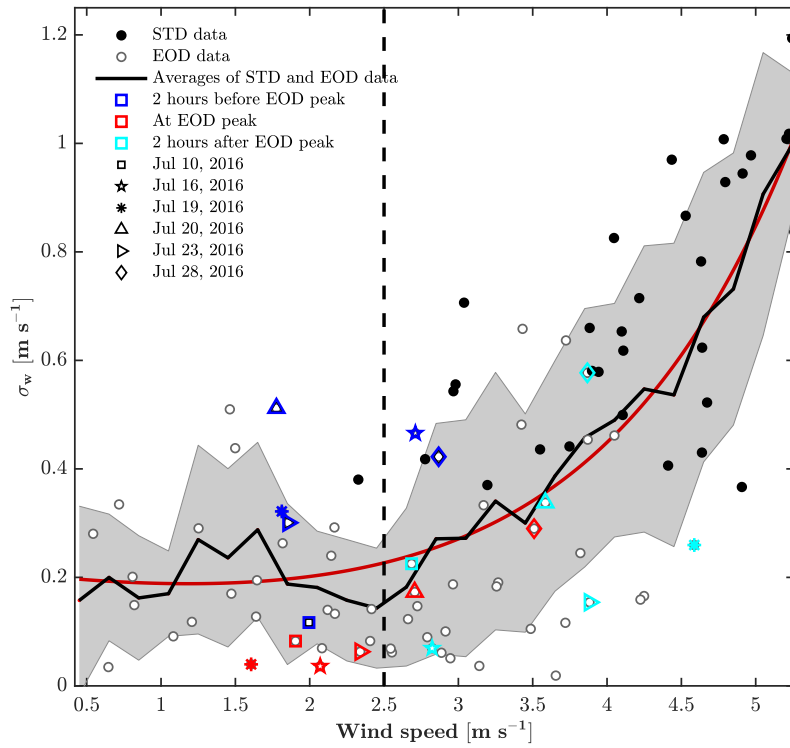


**Figure 4.** Dependence of  $\sigma_w$  on wind speed. Markers denote observations for the STD case (solid black circles) and the EOD case (open black circles). The data points of 2 hours before (blue), at (red), and 2 hours after the EOD peaks (cyan) are color coded with different symbols denoting different EOD-peak days (the turbulence data for Jul 4 2016 are missing). The bin-averaged (bin width is  $0.25 \text{ m s}^{-2}$ ) data (black line and the shaded area) and the fitting curve (red line) are also shown. The  $\sigma_w$  data measured at 34 m and wind speed data at 46 m are used in this figure.

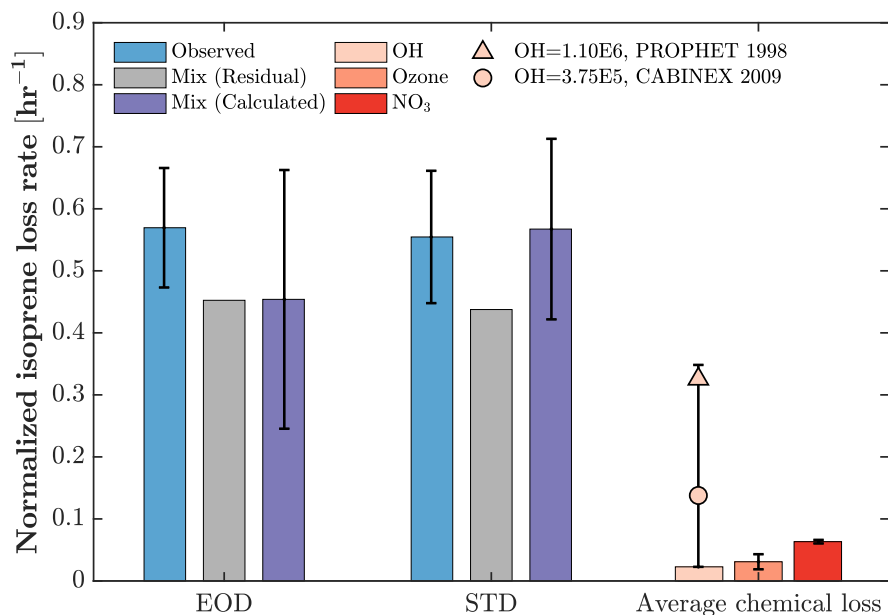


**Figure 5.** The loss rates of isoprene from 21:00 LT - 22:00 LT. Isoprene loss rate calculated from the observed isoprene mixing ratios (**blue**). Chemical loss with respect to hydroxyl radicals OH (**pink**), ozone (**orange**), and nitrate radicals NO<sub>3</sub> (**red**). Estimated isoprene loss rate due to vertical mixing (**grey**) as the differences between the observed (blue) and the chemical losses (pink, orange, and red). Estimated isoprene loss rate due to vertical mixing using the sonic anemometer data (Equation 4; **purple**). Isoprene chemical loss rates with respect to OH from previous campaigns at the same site (Faloon et al., 2001; Griffith et al., 2013) (**triangle and circle**). Error bars represent day-to-day variations. The error bar for OH also includes measurement uncertainty.

Figure 1.

Author Manuscript

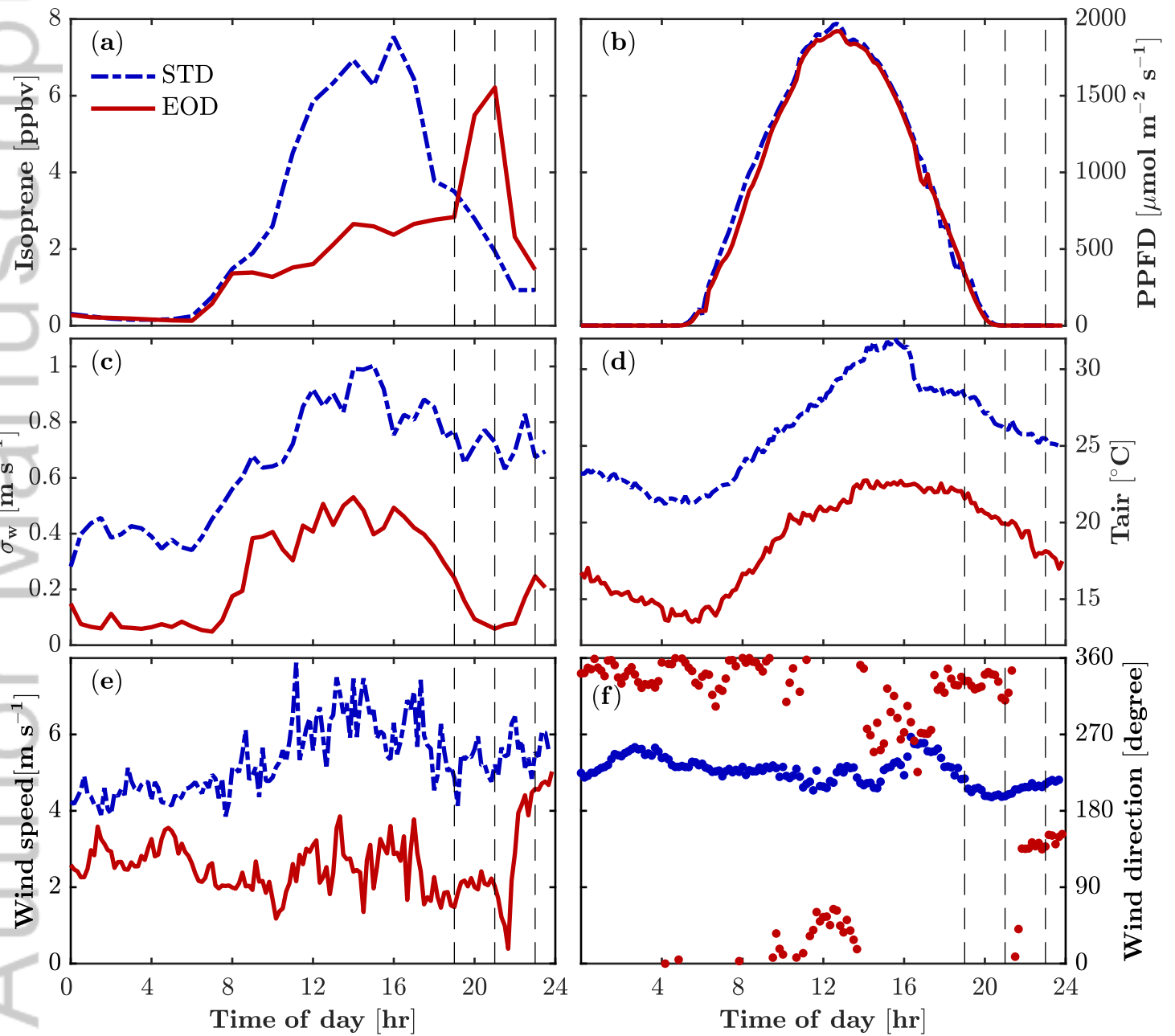




Figure 2.

Author Manuscript

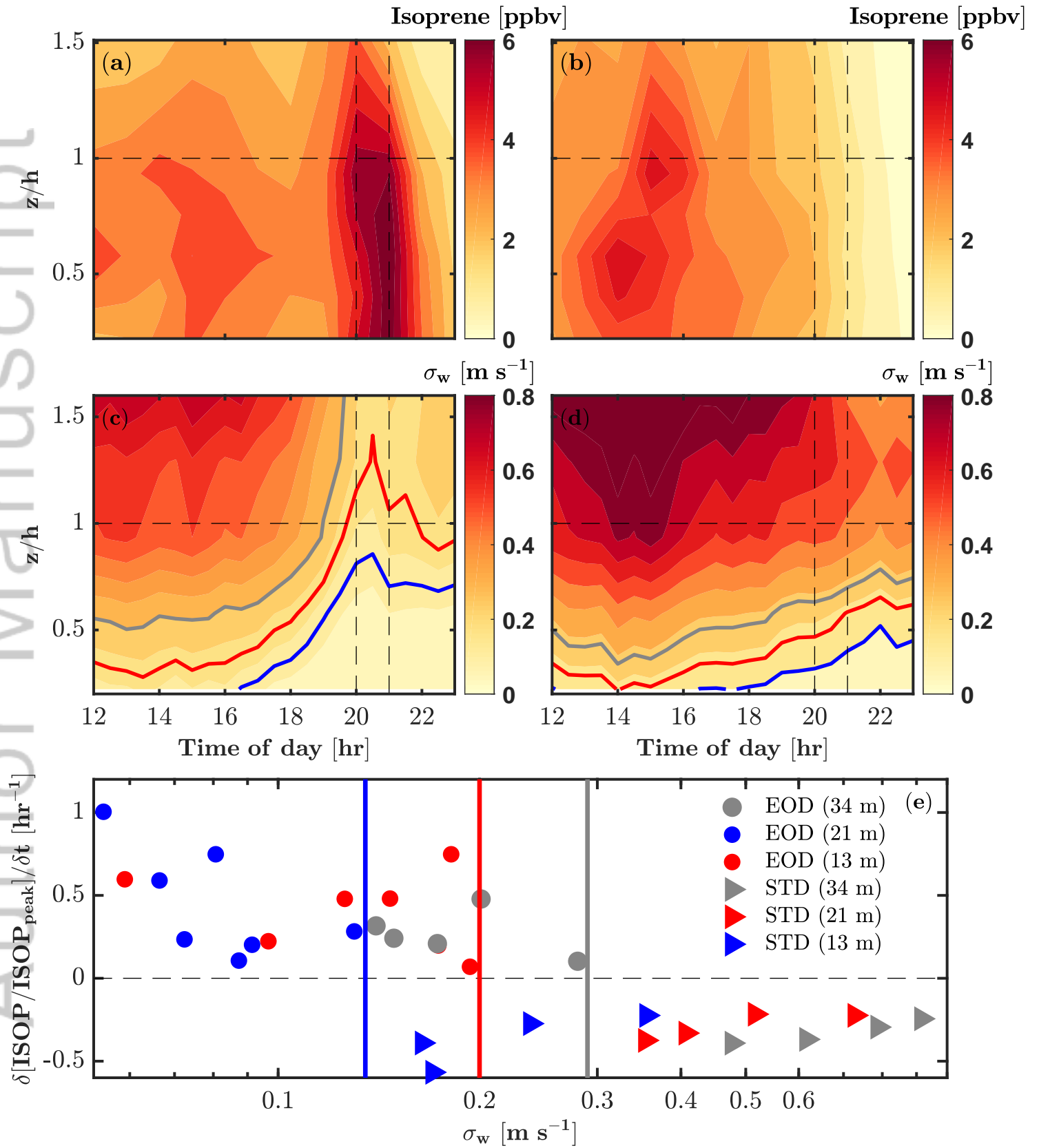


Figure 3.

Author Manuscript

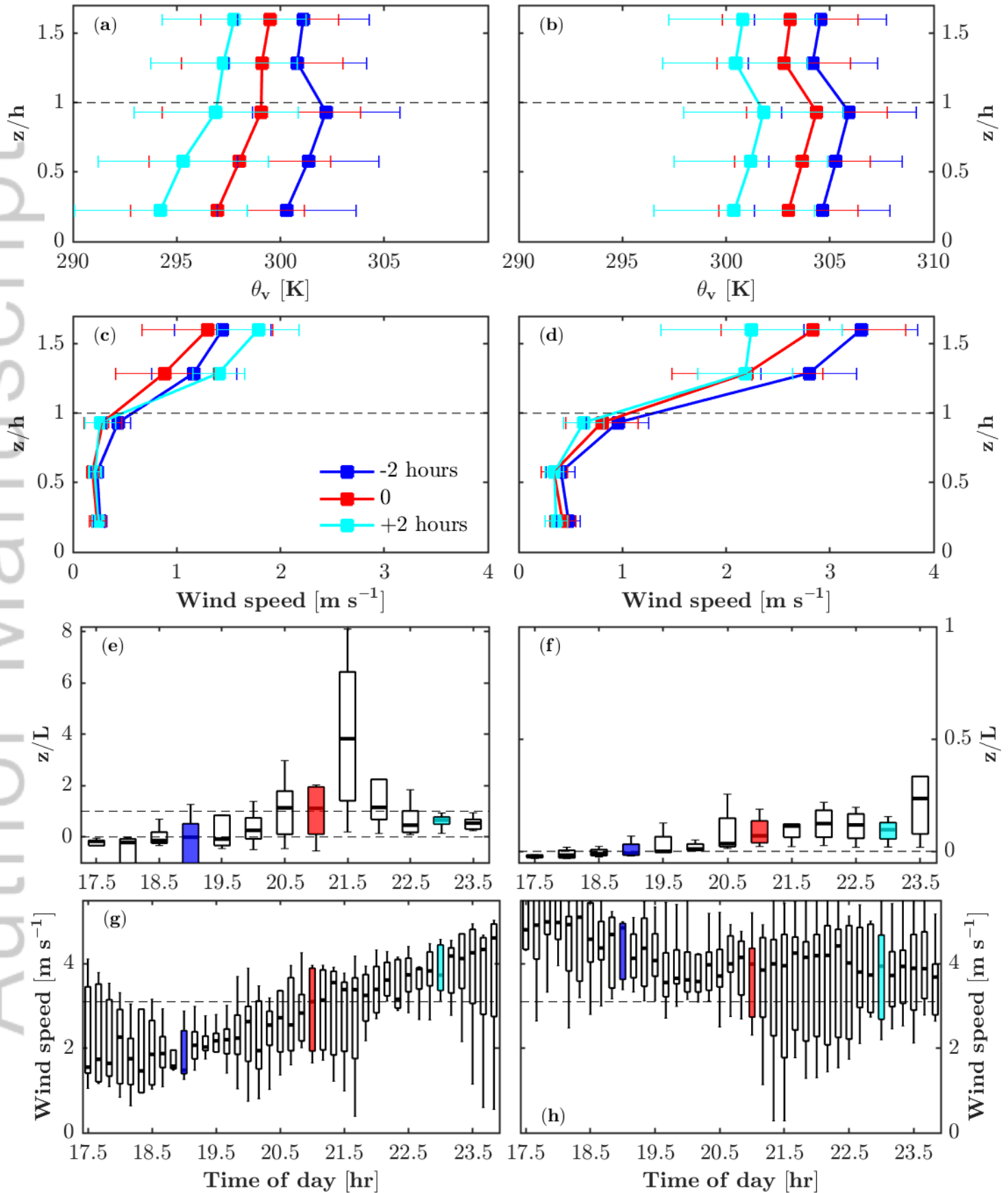


Figure 4.

Author Manuscript

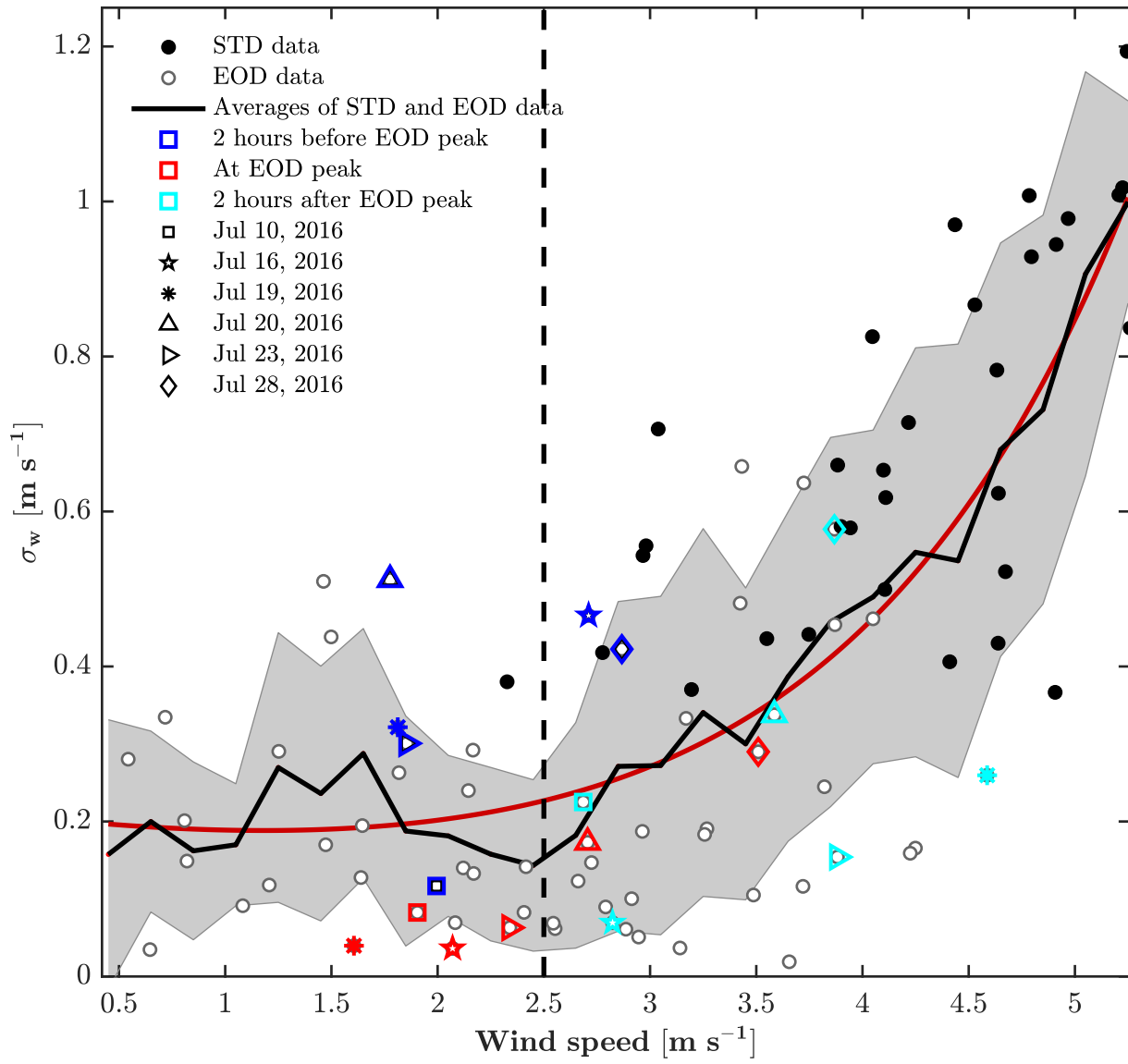


Figure 5.

Author Manuscript

